

Design, Structure–Activity Relationships, and In Vivo Evaluation of Potent and Brain-Penetrant Imidazo[1,2-*b*]pyridazines as Glycogen Synthase Kinase-3 β (GSK-3 β) Inhibitors

Richard A. Hartz,* Vijay T. Ahuja, Prasanna Sivaprakasam, Hong Xiao, Carol M. Krause, Wendy J. Clarke, Kevin Kish, Hal Lewis, Nicolas Szapiel, Ramu Ravirala, Sayali Mutualik, Deepa Nakmode, Devang Shah, Catherine R. Burton, John E. Macor, and Gene M. Dubowchik



Cite This: *J. Med. Chem.* 2023, 66, 4231–4252



Read Online

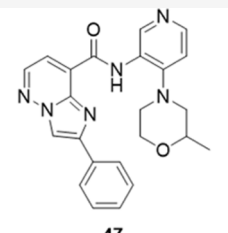
ACCESS |

Metrics & More

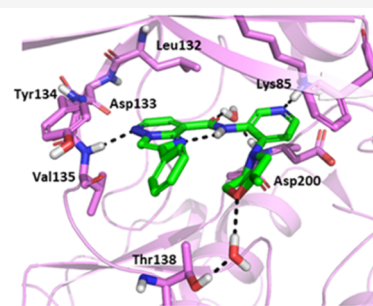
Article Recommendations

Supporting Information

ABSTRACT: Glycogen synthase kinase-3 (GSK-3) is a serine/threonine kinase that regulates numerous cellular processes, including metabolism, proliferation, and cell survival. Due to its multifaceted role, GSK-3 has been implicated in a variety of diseases, including Alzheimer's disease, type 2 diabetes, cancer, and mood disorders. GSK-3 β has been linked to the formation of the neurofibrillary tangles associated with Alzheimer's disease that arise from the hyperphosphorylation of tau protein. The design and synthesis of a series of imidazo[1,2-*b*]pyridazine derivatives that were evaluated as GSK-3 β inhibitors are described herein. Structure–activity relationship studies led to the identification of potent GSK-3 β inhibitors. In vivo studies with 47 in a triple-transgenic mouse Alzheimer's disease model showed that this compound is a brain-penetrant, orally bioavailable GSK-3 β inhibitor that significantly lowered levels of phosphorylated tau.



GSK-3 β IC₅₀ = 0.73 nM
pTau IC₅₀ = 58 nM
Active in pTau lowering model



In vivo studies with 47 in a triple-transgenic mouse Alzheimer's disease model showed that this compound is a brain-penetrant, orally bioavailable GSK-3 β inhibitor that significantly lowered levels of phosphorylated tau.

INTRODUCTION

Alzheimer's disease is a neurodegenerative disorder resulting in cognitive impairment and progressive loss of memory and is the most common form of dementia.¹ Approximately 5.8 million Americans are living with Alzheimer's disease, and this number is expected to grow to 14 million by 2050.² The number of people affected worldwide by this disease is projected to grow from 53 million in 2018 to 88 million by 2050.³ It is thought that Alzheimer's disease begins 20 years or more before symptoms arise, during which time changes in the brain of the affected person are unnoticeable.⁴ After years of brain changes, individuals begin to experience noticeable symptoms, such as memory loss and language problems, and as the disease progresses, patients experience spatial disorientation, personality changes, and additional psychiatric symptoms that prevent them from functioning independently. These changes are accompanied by the death of neurons and damage to brain tissue. The two hallmark pathologies of Alzheimer's disease that are underlying major contributors to the deleterious brain changes are the accumulation of extracellular β -amyloid ($A\beta$) plaques and the presence of intracellular neurofibrillary tangles (NFTs) composed of hyperphosphorylated tau protein.⁵ Despite many years of research and numerous clinical trials, the discovery of effective therapies

for the treatment of Alzheimer's disease continues to be a major unmet medical need.

Glycogen synthase kinase-3 (GSK-3) is a constitutively active, proline-directed serine/threonine kinase that was originally identified in 1980 for its role as an enzyme involved in the regulation of glycogen metabolism.⁶ Since then, GSK-3 has been found to be widely distributed throughout the body with around 100 proteins proposed as substrates for this enzyme.⁷ GSK-3 regulates many metabolic, signaling, and structural proteins and maintains control over a broad array of transcription factors. It is involved in the regulation of a diverse range of cellular functions, such as metabolism, proliferation, cell survival, and apoptosis,⁸ and is an important regulator of the Wnt signaling pathway.⁹ GSK-3 has been implicated in a variety of diseases including Alzheimer's disease,^{10–15} type 2 diabetes,^{15,16} cancer,^{15,17} mood disorders,¹⁸ and myocardial disease.¹⁹ GSK-3 exists as two isoforms designated as GSK-3 α (51 kDa) and GSK-3 β (47 kDa). These isoforms share greater

Received: January 23, 2023

Published: March 9, 2023



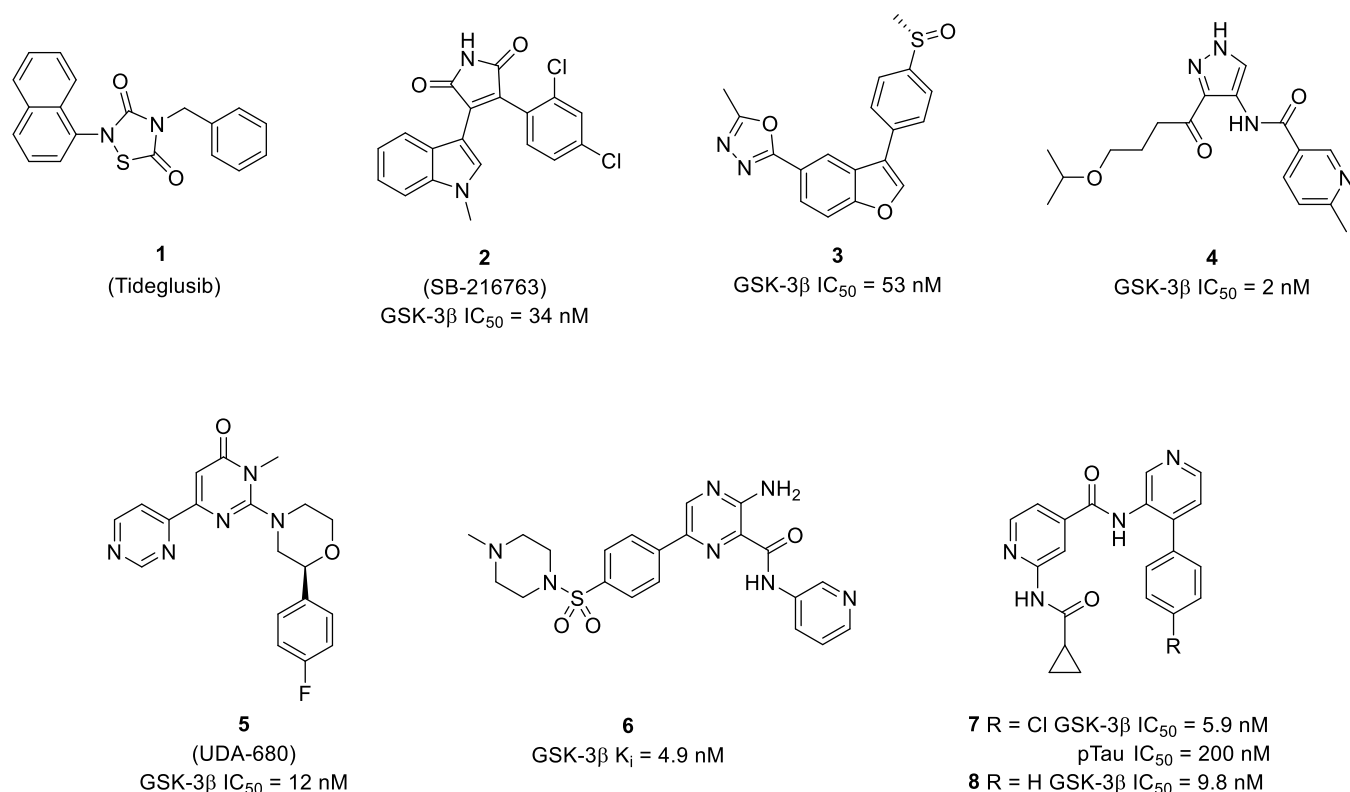


Figure 1. Representative GSK-3 β inhibitors.

than 98% identity within their respective catalytic domains and 84% overall identity, differing primarily in the Gly-rich segment in the N-terminal region of GSK-3 α .²⁰ A splice variant of GSK-3 β (GSK-3 β 2), which contains an additional 13 amino acid segment on the C-terminal side of the catalytic domain, has also been identified.²¹ Both GSK-3 α and GSK-3 β are ubiquitously expressed in tissues, with particularly high expression levels present in the central nervous system (CNS).^{22,23} The predominant isoform found in most areas of the CNS is GSK-3 β .²⁴

GSK-3 has been linked to the formation of NFTs composed of tau protein and to A β accumulation. Tau is a microtubule-associated phosphoprotein found predominantly in neurons where it binds to and stabilizes microtubules. Phosphorylation of tau is normally a rapid and reversible process mediated by the action of protein kinases and phosphatases.^{11,25} Overactivation of GSK-3 β results in the hyperphosphorylation of tau proteins. The hyperphosphorylated tau disengages from microtubules leading to microtubule depolymerization and destabilization with undesirable effects on intracellular structures and transport mechanisms.²⁶ The formation of paired helical fragments composed of uncomplexed, hyperphosphorylated tau, and their subsequent aggregation leads to the formation of intracellular NFTs and a subsequent increase in β -amyloid production. Overactivity of GSK-3 may also promote the activity of β - and γ -secretases resulting in A β accumulation and formation of A β plaque.

Lithium is a well-tolerated drug that has been used for the treatment of bipolar disorders²⁷ and has been used extensively in many pharmacological studies. It inhibits GSK-3 β directly by competing with magnesium and indirectly by increasing inhibitory phosphorylation of GSK-3 β at the Ser9 site.²⁸ When phosphorylated at Ser9, the N-terminal domain of GSK-3 β acts

as a pseudosubstrate, blocking the access of substrates to the catalytic site.²⁹ It was found that a reduction of tau phosphorylation in vivo occurred when triple-transgenic mice overexpressing human mutant tau were treated with lithium chloride.³⁰ In a separate study, administration of lithium chloride to JNPL3 mice resulted in significantly reduced levels of tau phosphorylation at putative GSK-3-directed sites, including Ser202 and Ser396/404, which are known to be hyperphosphorylated in Alzheimer's disease, and a reduction in levels of aggregated, insoluble tau was also observed.³¹ Moreover, evidence obtained from brain autopsies of Alzheimer's disease patients revealed the presence of increased levels of GSK-3 compared to age-matched control samples.²² Taken together, these studies support the potential for GSK-3 inhibitors as agents for the treatment of Alzheimer's disease.

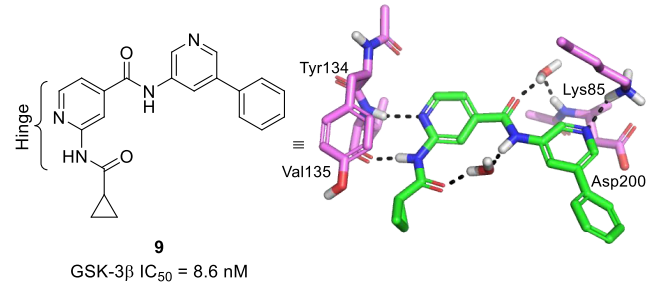
Numerous pharmaceutical companies and academic research groups have discovered a group of structurally diverse small-molecule GSK-3 β inhibitors, and multiple review articles have been published on this topic.^{3,14,15,32–38} GSK-3 β inhibitors have been investigated for the potential treatment of Alzheimer's disease and cancer, as potential antidiabetic agents, and for other therapeutic indications. GSK-3 inhibitors have also recently been investigated as agents for cancer immunotherapy.^{39,40} A group of selected GSK-3 β inhibitors that were evaluated for the potential treatment of Alzheimer's disease is shown in Figure 1. Tideglusib (1), a non-ATP-competitive GSK-3 inhibitor, completed phase II studies for Alzheimer's disease.⁴¹ ATP-competitive GSK-3 β inhibitors have also been investigated for the potential treatment of Alzheimer's disease. Intravenous administration of arylmaleimide 2 (SB-216763), an early GSK-3 β inhibitor, at a dose of 30 mg/kg reduced tau hyperphosphorylation in a rat brain model.⁴² A brain-penetrant benzofuran-based compound (3)

was also reported to reduce tau phosphorylation at GSK-3-directed sites and improve memory and cognitive deficits in the Y-maze and in novel object recognition tests in the transgenic Alzheimer's disease mouse model.^{43,44} It was found that oral administration of pyrazole **4** to rats significantly reduced tau phosphorylation at several GSK-3-directed sites. In addition, chronic oral administration of **4** significantly reduced levels of aggregated tau in old JNPL3 mice.⁴⁵ In vivo studies in mice with compound **5** (UDA-680) showed that it, as well as a follow-up analogue from the same chemotype, significantly inhibited tau phosphorylation at a dose of 30 mg/kg (po).^{46,47} 2-Aminopyridine **6** was reported to exhibit good selectivity against a panel of 26 kinases and inhibit tau phosphorylation in an assay with cells that were engineered to express tau protein.⁴⁸ Early on in our research program, systematic exploration of the chemical space around a pyrrolopyridinone core led to highly potent GSK-3 β inhibitors.⁴⁹ Subsequent structure–activity relationship (SAR) studies resulted in the discovery of isonicotinamide-based GSK-3 β inhibitor **7**. Isonicotinamide **7** showed excellent kinase selectivity for GSK-3 in an Ambit panel of almost 400 kinases and significantly lowered tau phosphorylation in a triple-transgenic mouse Alzheimer's disease model when administered orally at doses of 10 and 30 mg/kg.⁵⁰

While conducting in-house SAR studies on a series of isonicotinamide-based GSK-3 β inhibitors leading to the identification of **7**, an X-ray co-crystal structure of **9** complexed with GSK-3 β was obtained.⁵¹ A water-bridging hydrogen bond between the cyclopropyl carboxamide carbonyl and the upper amide NH was observed in this X-ray co-crystal structure (Figure 2A), which may help to predispose the molecule to energetically favor the bioactive conformation. It was found that the cyclopropyl carboxamide moiety was one of the most preferred amides in this chemotype for balancing potency and metabolic stability. However, when **8**, an analogue of **7**, was incubated in mouse serum at 37 °C, 24% cleavage of the cyclopropyl carboxamide group was observed over 3 h, although in human serum only trace levels of cleavage were detected.⁵⁰ In addition, due to a report suggesting the potential for idiosyncratic toxicity if cyclopropane carboxylic acid is liberated from the parent compound in vivo,⁵² we were interested in replacing the cyclopropyl carboxamide moiety in the isonicotinamide chemotype with other amides or alternative substituents.^{51,53} We also envisioned that a heterocyclic tieback of the lower amide (represented by the red dashed line in Figure 2B), wherein a nitrogen replaces the carbonyl oxygen, would prefer the bioactive conformation by forming an internal hydrogen bond (represented by the blue dashed line in Figure 2B). With this in mind, the imidazo[1,2-*b*]pyridazine ring system appeared to be an attractive heterocyclic scaffold for the design of GSK-3 β inhibitors. Furthermore, an analysis of the dipole interactions between the amide and neighboring imidazo[1,2-*b*]pyridazine ring system indicates that the desired bioactive conformation has a favorable alignment of dipoles as illustrated by the blue arrows (Figure 2B).

Substitution at either the 3- or 2-position on the imidazo[1,2-*b*]pyridazine scaffold was envisioned as shown in Figure 3. The subtype 1 imidazo[1,2-*b*]pyridazine scaffold preserves both classic hydrogen bond acceptor and donor interactions with the hinge region of GSK-3 β that are present in isonicotinamides **7**–**9** (the pyridyl nitrogen and cyclopropyl carboxamide NH group) by incorporating an alkylamine

A



B

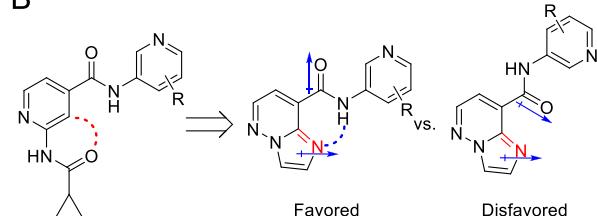


Figure 2. (A) X-ray co-crystal structure of **9** in the kinase domain of GSK-3 β (PDB ID: 8DJD) with hydrogens added from a molecular modeling program.⁵⁴ The ligand is rendered as a stick model with green carbon atoms and hydrogen bonds are shown as black dashed lines. The amino acid residues involved in hydrogen bonding with the ligand are displayed as sticks. A water-bridging hydrogen bond was observed between the cyclopropylamide carbonyl and the pyridyl amide NH in **9**. The figure was made using PyMOL.⁵⁵ (B) Rationale for the imidazo[1,2-*b*]pyridazine-based GSK-3 β inhibitor scaffold. The red dashed line represents a proposed tieback to form a five-membered ring. The blue dashed line represents an internal hydrogen bond. The desired amide conformation has a favorable alignment of dipoles with the neighboring imidazo[1,2-*b*]pyridazine ring system as indicated by the blue arrows.

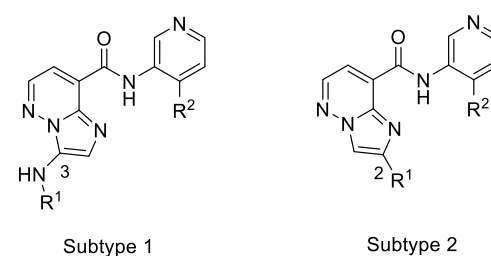
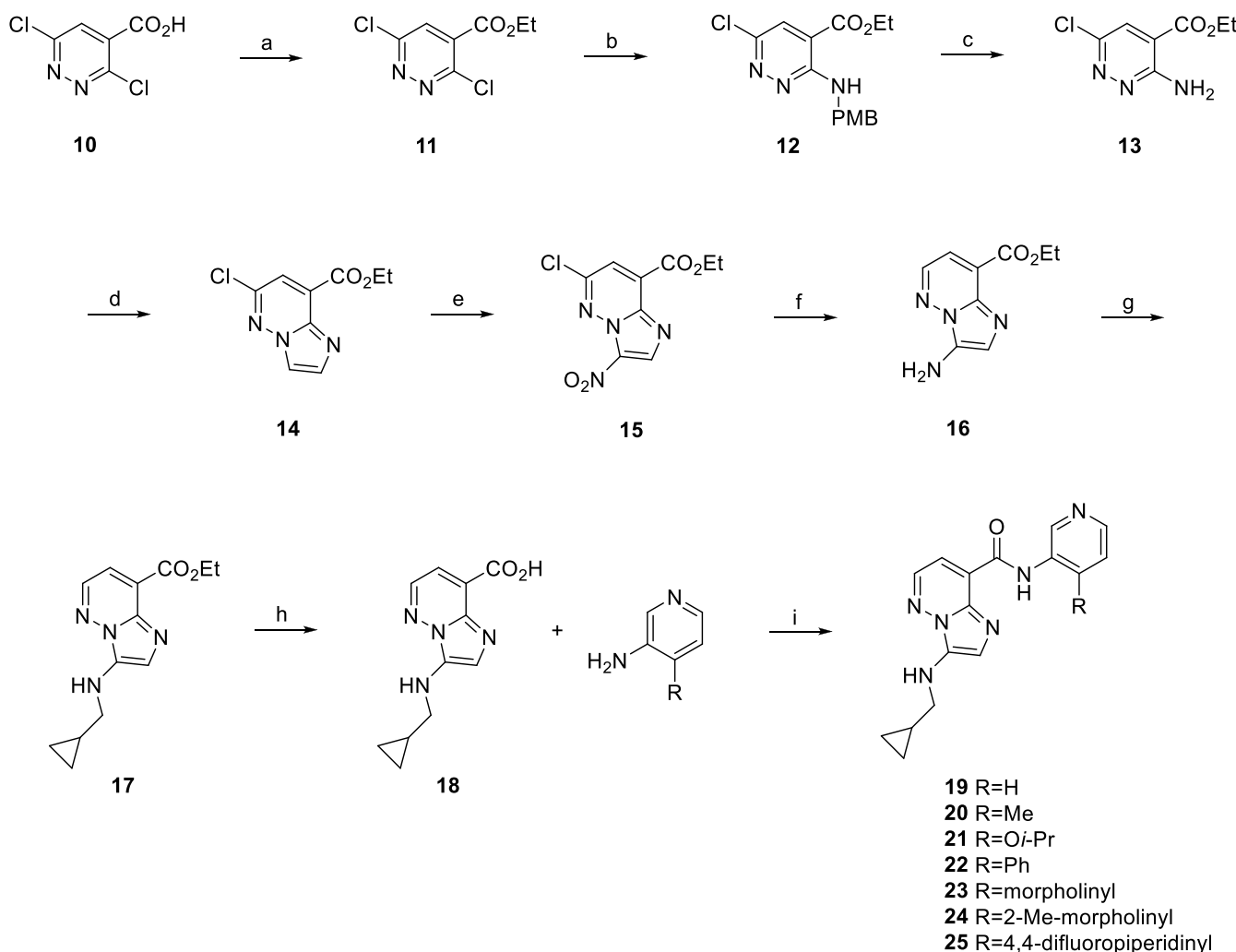


Figure 3. Proposed imidazo[1,2-*b*]pyridazine-based GSK-3 β inhibitors.

substituent at the 3-position of the imidazo[1,2-*b*]pyridazine ring system. Since these inhibitors were intended for use as agents for the treatment of Alzheimer's disease, brain penetrance was an important consideration. In the subtype 2 imidazo[1,2-*b*]pyridazine scaffold, the hinge-binding hydrogen bond donor group was removed, leaving only the hydrogen bond acceptor, which may lead to improved brain penetration.^{56,57} In this case, substitution at the 2-position of the imidazo[1,2-*b*]pyridazine ring system was planned. The synthesis, SAR, and in vivo evaluation of imidazo[1,2-*b*]pyridazine-based GSK-3 β inhibitors are described herein.

■ CHEMISTRY

The route to synthesize subtype 1 imidazo[1,2-*b*]pyridazine analogues that contain a cyclopropylmethyl amine substituent at the 3-position of the imidazo[1,2-*b*]pyridazine ring system is

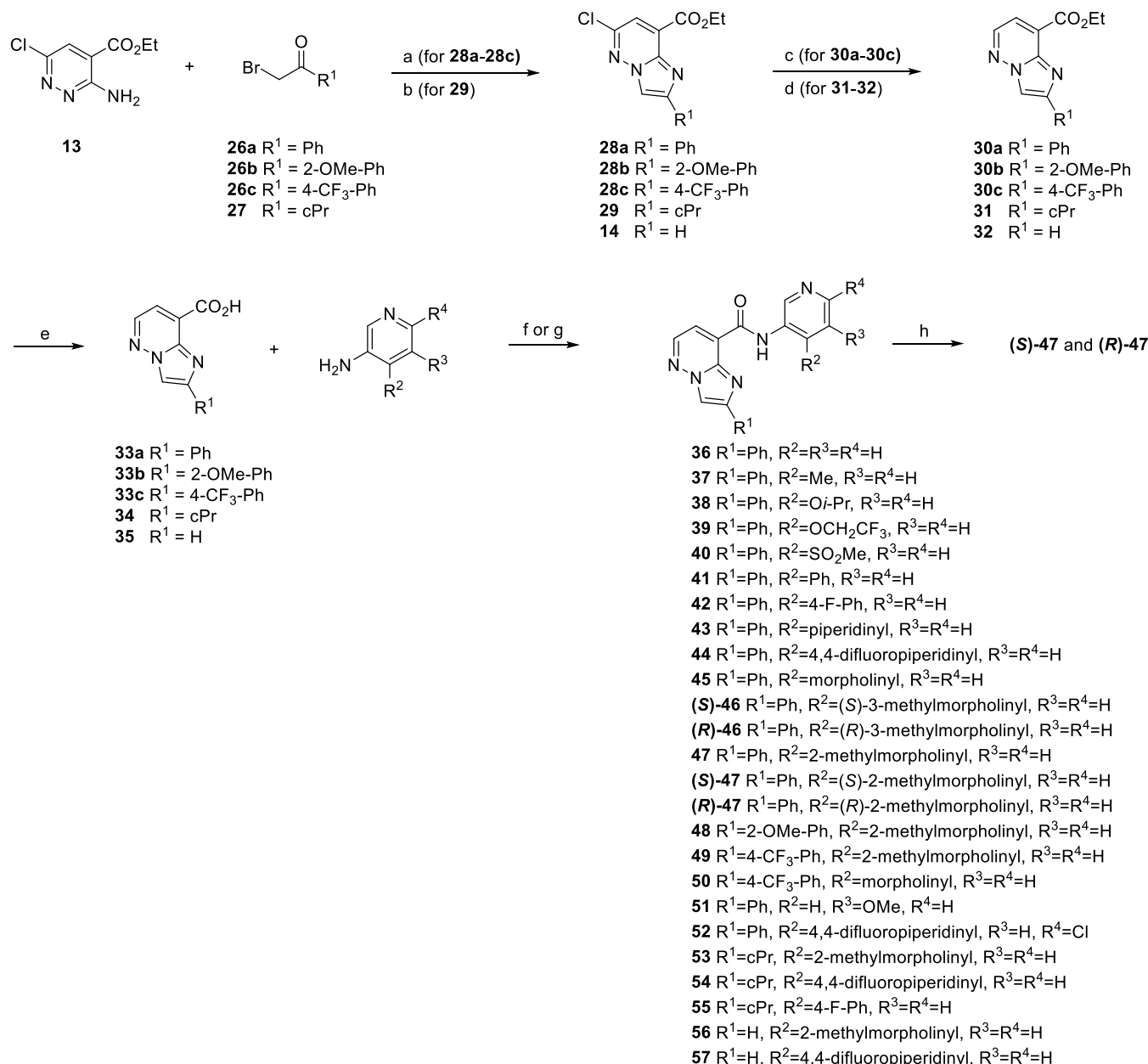
Scheme 1. General Synthetic Route for the Preparation of 3-Substituted Imidazo[1,2-*b*]pyridazines^a

^aReagents and conditions: (a) EtOH, EDC, DMAP, tetrahydrofuran (THF), 22 °C, 16 h, 77%; (b) 4-methoxybenzylamine, *i*-Pr₂NEt, 1,4-dioxane, 80 °C, 20 min, 86%; (c) TFA, reflux, 3 h, 64%; (d) chloroacetaldehyde (50% in H₂O), *i*-PrOH, 80 °C, 4 h, 67%; (e) fuming HNO₃, H₂SO₄, 0–22 °C, 5 h, 67%; (f) H₂, 10% Pd/C, Et₃N, EtOH/dimethylformide (DMF), 3 atm (45 psi), 4 h, 82%; (g) cyclopropanecarboxaldehyde, NaBH₃CN, HOAc, MeOH, 22 °C, 2 h, 50%; (h) LiOH·H₂O, THF/H₂O, 22 °C, 2 h, 89–92%; (i) HATU, *i*-Pr₂NEt, DMF, 22 °C, 4 h, 16–46%.

shown in Scheme 1.⁵⁸ Ester formation was carried out by stirring a solution of 3,6-dichloropyridazine-4-carboxylic acid (**10**) in EtOH in the presence of 1-ethyl-3-(3-dimethylaminopropyl)carbodiimide (EDC) and 4-dimethylaminopyridine (DMAP) to provide ethyl 3,6-dichloropyridazine-4-carboxylate (**11**). This product was heated in the presence of 4-methoxybenzylamine resulting in S_NAr-type displacement of the 3-chloro substituent to form intermediate **12**. The resultant *p*-methoxybenzyl group in **12** was removed by heating with trifluoroacetic acid (TFA) to furnish ethyl 3-amino-6-chloropyridazine-4-carboxylate (**13**). Cyclization of **13** was achieved by heating with chloroacetaldehyde to afford the imidazo[1,2-*b*]pyridazine ring system (**14**). Nitration of **14** at the 3-position of the heterocyclic ring system furnished intermediate **15** in 67% yield. Reduction of the nitro group to the amine along with removal of the chloride was accomplished by hydrogenation of **15** at 3 atm (45 psi) in the presence of 10% palladium on carbon to afford 3-amino-substituted imidazo[1,2-*b*]pyridazine **16** in good yield. *N*-Alkylation of **16** via reductive amination with cyclopropanecarboxaldehyde furnished intermediate **17** in 50% yield.

Subsequent hydrolysis of the ethyl ester with LiOH afforded carboxylic acid intermediate **18** in high yield. Carboxylic acid **18** was then coupled with 3-aminopyridines in the presence of hexafluorophosphate azabenzotriazole tetramethyl uronium (HATU) to afford imidazo[1,2-*b*]pyridazine products **19–25**.

A series of subtype 2 imidazo[1,2-*b*]pyridazine analogues containing either a phenyl or cyclopropyl substituent at the 2-position of the imidazo[1,2-*b*]pyridazine ring system was synthesized as shown in Scheme 2. In this route, amino-pyridazine **13** was heated in the presence of commercially available 2-bromoacetophenone (**26a**) to furnish 2-phenyl-substituted imidazo[1,2-*b*]pyridazine **28a**. Removal of the chloro substituent in **28a** was carried out by hydrogenation in the presence of 10% palladium on carbon to furnish imidazo[1,2-*b*]pyridazine **30a**. Compounds **30b**, **30c**, and **31** were prepared in a similar manner as **30a**. Hydrolysis of the ethyl ester with LiOH afforded carboxylic acid intermediates **33a–33c** and **34** in high yield. The carboxylic acid intermediates were coupled with 3-aminopyridines to furnish the final products **36–55**.⁵⁹ The 3-aminopyridines were selected on the basis of SAR we developed in the

Scheme 2. General Synthetic Route for the Preparation of 2-Substituted Imidazo[1,2-*b*]pyridazines^a

^aReagents and conditions: (a) 26a, 26b, or 26c, DMF, 60 °C, 4 h, 38–67%; (b) 27, 1,4-dioxane, 90 °C, 4 h, 41%; (c) H₂, 10% Pd/C, CHCl₃/EtOH, 1 atm, 14 h, 43–52%; (d) H₂, 10% Pd/C, EtOH, 1 atm, 20 min (for 31) or 15 min (for 32), 78–93%; (e) LiOH·H₂O, THF/H₂O, 22 °C, 2 h, 76–99%; (f) HATU, i-Pr₂NEt, DMF, 22 °C, 6 h, 23–63% (for 36–39, 41–48, and 51–57); (g) (COCl)₂, DMF, 22 °C, 1 h then Et₃N, DMAP, 3-aminopyridines, CH₂Cl₂, 22 °C, 4 h, 12–30% (for 40, 49, and 50); (h) enantiomers of 47 were separated by chiral SFC using a ChiralPak AS-H column, 35% for (S)-47; 35% for (R)-47.

isonicotinamide series.^{50,51} The enantiomers of imidazo[1,2-*b*]pyridazine 47 were initially separated by chiral chromatography (Chiraldak AS-H column) resulting in material with >99% ee. Compounds (S)-47 and (R)-47 were later resynthesized from enantiomerically pure starting materials to assign the stereochemistry of each enantiomer from the chiral separation. Two analogues were also synthesized without a substituent at the 2-position of the imidazo[1,2-*b*]pyridazine ring. Preparation of these analogues was conducted by subjecting 6-chloroimidazo[1,2-*b*]pyridazine 14 to hydrogenation at 1 atm in the presence of 10% palladium on carbon to furnish intermediate 32. In the case of 14, the hydro-

genation reaction was closely monitored since extended reaction times resulted in partial reduction of the imidazo[1,2-*b*]pyridazine ring system. A reaction time of only 15 min accompanied by rapid stirring of the reaction mixture resulted in complete dechlorination of 14. Hydrolysis of ethyl ester 32 with LiOH afforded 35. Subsequent amide formation afforded final products 56 and 57.

RESULTS AND DISCUSSION

Structure–Activity Relationships and X-ray Crystallography. The potency of each compound was measured in GSK-3β/α competition assays with a fluorescently labeled

small molecule at its K_d to determine the GSK-3 β/α IC₅₀ values. The SAR at the 4-position of the pyridyl ring was explored in the subtype 1 imidazo[1,2-*b*]pyridazine-based series and the results are shown in Table 1. Compound 19 had

Table 1. GSK-3 β and GSK-3 α Inhibitory Activity for Compounds 19–25

cmpd	R	GSK-3 β IC ₅₀ (nM) ^a	GSK-3 α IC ₅₀ (nM) ^a
19	H	220 ± 40	510 ± 390
20	Me	63 ± 18	30 ^c
21	O <i>i</i> Pr	6.7 ± 1.9	3.4 ^c
22	Ph	3.5 ± 0.6 ^b	2.0 ± 0.3
23		9.0 ± 5.1	1.4 ± 0.2
24		5.2 ± 3.9	1.6 ± 1.0
25		0.87 ± 0.44 ^b	1.4 ± 1.6 ^b

^aValues are means of two determinations unless indicated otherwise.

^bValue is the mean of at least three determinations ± standard deviation (SD). ^cValue is the result of a single determination.

an IC₅₀ value of 220 nM in the GSK-3 β enzyme assay. A 3.5-fold improvement in potency was observed when the pyridine was substituted with a methyl group at the 4-position (20), and an additional 10-fold improvement in potency occurred when the methyl group was replaced with an isopropyl ether (compare 21 to 20). Additional analogues with either a phenyl group (22) or a 6-membered ring heterocycle (23–24) were similar in potency to compound 21. The 4,4-difluoropiperidinyl analogue (25) was the most potent analogue in this group (GSK-3 β IC₅₀ = 0.87 nM). In general, the potencies of the compounds shown in Table 1 for GSK-3 β and GSK-3 α were within 3-fold of each other and are not considered to be isoform selective.

An X-ray co-crystal structure of compound 22 bound in the catalytic domain of GSK-3 β was obtained and is shown in Figure 4. The protein crystallizes as a dimer with similar interactions of ligands in each of the binding pockets. The sp² nitrogen in the six-membered ring of the imidazo[1,2-*b*]pyridazine and the amino group of the cyclopropylmethyl amine substituent form hydrogen bonds with Val135 (2.5 and 2.1 Å, respectively) in the hinge region of the catalytic domain of GSK-3 β . The sp² nitrogen of the pyridine moiety forms a hydrogen bond with the Lys85 amine (1.9 Å). A water-mediated hydrogen bond was observed between the amide carbonyl and the backbone NH of Asp200. The phenyl group occupies the ribose-binding site, and this region of the molecule provided a means to optimize the potency of this chemotype due to favorable van der Waals contacts with the protein. The improved potency of analogues 21–25 compared

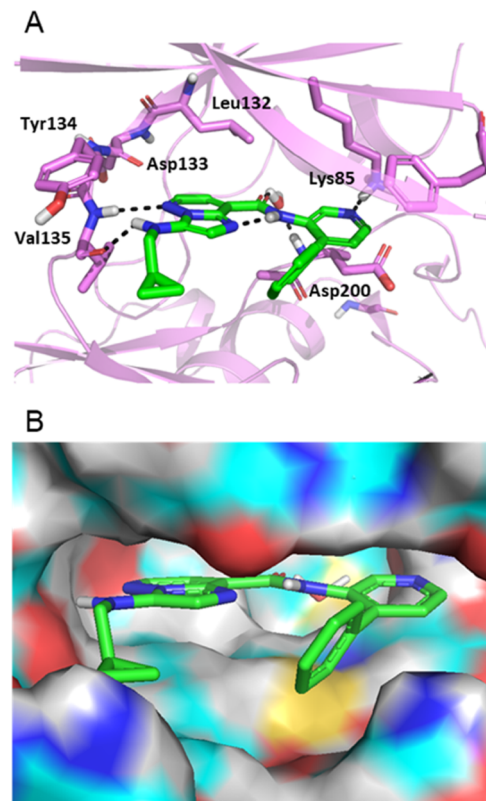
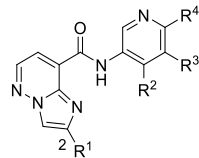


Figure 4. X-ray co-crystal structure of 22 bound in the kinase domain of GSK-3 β (PDB ID: 8DJE) with hydrogens added from a molecular modeling program.⁵⁴ The ATP-binding site is shown. (A) Ligand is rendered as a stick model with green carbon atoms and hydrogen bonds are shown as black dashed lines. Residues involved in interactions with the ligand are displayed as sticks. The phenyl group occupies the ribose-binding site. (B) Surface representation of the protein with 22 bound to the ATP-binding site of GSK-3 β (bottom). Figures are made using PyMOL.⁵⁵

to compounds 19 and 20 in Table 1 can be attributed to favorable interactions of the respective substituents at the 4-position of the pyridyl ring with the protein in the ribose-binding site. An internal hydrogen bond was observed between the amide NH and the N¹ nitrogen in the imidazo[1,2-*b*]pyridazine ring system. A surface representation of the protein with 22 bound to the ATP-binding site of GSK-3 β is shown in Figure 4B.

The SAR at the 4-position of the pyridyl ring was explored in combination with either a phenyl or cyclopropyl substituent at the 2-position of the subtype 2 imidazo[1,2-*b*]pyridazine ring system and the results are shown in Tables 2 and 3. A comparison between the parent unsubstituted pyridyl analogues 19 and 36 shows that the latter is 11-fold more potent than 19 (GSK-3 β IC₅₀ = 20 vs 220 nM, respectively). We found that phenyl-substituted analogues at R¹ in this series were ~5- to 20-fold more potent than the corresponding analogues in Table 1 (compare 37, 38, 45, and 47 to 20, 21, 23, and 24, respectively). Incorporation of a methyl group at the 4-position of the pyridyl ring (37) resulted in a compound with a GSK-3 β IC₅₀ value of 3.5 nM. Compounds with moderately larger groups (38–40) had GSK-3 β IC₅₀ values of ~1 nM or less. Analogues containing a phenyl group at R² (41 and 42) were shown to be potent (GSK-3 β IC₅₀ = 3.6 and 1.6 nM, respectively). Furthermore, replacement of phenyl with

Table 2. GSK-3 β and GSK-3 α Inhibitory Activity for Compounds 36–52

cmpd	R ¹	R ²	R ³	R ⁴	GSK-3 β IC ₅₀ (nM) ^a	GSK-3 α IC ₅₀ (nM) ^a
36	Ph	H	H	H	20 ± 4 ^b	6.7 ± 1.5 ^b
37	Ph	Me	H	H	3.5 ± 1.0	0.80 ± 0.22
38	Ph	O <i>i</i> Pr	H	H	0.70 ± 0.08	0.41 ± 0.10
39	Ph	OCH ₂ CF ₃	H	H	0.29 ± 0.04 ^b	0.09 ± 0.04 ^b
40	Ph	SO ₂ Me	H	H	1.5 ± 1.0	0.40 ^c
41	Ph	Ph	H	H	3.6 ± 0.7	1.1 ± 0.6
42	Ph	4-F-Ph	H	H	1.6 ± 0.2	1.1 ± 0.5
43	Ph		H	H	1.1 ± 0.6	0.24 ± 0.03
44	Ph		H	H	0.37 ± 0.04	0.22 ± 0.10
45	Ph		H	H	0.42 ± 0.01	0.21 ± 0.09
(S)-46	Ph		H	H	0.32 ± 0.06	0.32 ± 0.05
(R)-46	Ph		H	H	3.4 ± 2.0	1.0 ± 0.3
47	Ph		H	H	0.73 ± 0.27 ^b	0.35 ± 0.13
(S)-47	Ph		H	H	0.13 ± 0.03 ^b	0.10 ± 0.01 ^b
(R)-47	Ph		H	H	0.82 ± 0.16	0.34 ^c
48	2-OMe-Ph		H	H	0.57 ± 0.26	0.38 ± 0.06
49	4-CF ₃ -Ph		H	H	1.4 ± 0.1	0.57 ^c
50	4-CF ₃ -Ph		H	H	0.78 ± 0.04	0.23 ± 0.02
51	Ph	H	OMe	H	37 ± 9	7.5 ± 0.2
52	Ph		H	Cl	14 ± 3	2.9 ± 0.4

^aValues are means of two determinations unless indicated otherwise. ^bValue is the mean of at least three determinations ± SD. ^cValue is the result of a single determination.

six-membered ring heterocycles provided highly potent compounds, most with GSK-3 β IC₅₀ values in the subnanomolar range (43–47). After separation of compound 47 into its enantiomers by chiral chromatography, the results show that (S)-47 is ~6-fold more potent than (R)-47. The addition of either an *ortho* methoxy or *para* trifluoromethoxy substituent on the phenyl ring at R¹ was tolerated (compare 48 and 49 to 47 and compare 50 to 45). Substitution at R³ and R⁴ of the pyridine moiety was also investigated. The analogue

with a methoxy group at R³ was nearly 2-fold less potent than the unsubstituted pyridine analogue (compare 51 to 36). Chloro substitution at R⁴ resulted in a 35-fold decrease in potency (compare 52 to 44). Similar to what was observed with the subtype 1 imidazo[1,2-*b*]pyridazines (Table 1), the GSK-3 β and GSK-3 α potencies of the compounds shown in Table 2 were generally within 3- to 4-fold of each other.

Replacement of the phenyl group at the 2-position of the imidazo[1,2-*b*]pyridazine with a cyclopropyl group was also

Table 3. GSK-3 β and GSK-3 α Inhibitory Activity for Compounds 53–57

cmpd	R ¹	R ²	GSK-3 β IC ₅₀ (nM) ^a	GSK-3 α IC ₅₀ (nM) ^a
53	cPr		2.6 ± 0.7	0.8 ± 0.3
54	cPr		0.43 ± 0.07 ^b	0.18 ± 0.03 ^b
55	cPr	4-F-Ph	1.9 ± 0.5 ^b	0.44 ± 0.16 ^b
56	H		7.0 ± 3.3	3.2 ± 1.3
57	H		4.6 ± 2.0	2.4 ± 0.4

^aValues are means of two determinations unless indicated otherwise.

^bValue is the mean of at least three determinations ± SD.

investigated. As shown in **Table 3**, these analogues were generally comparable in potency to the corresponding compounds with a phenyl group at this position (compare **54** and **55** to **44** and **42**, respectively). Compound **53** was slightly less potent than **47**. Compounds **53** and **54** were comparable in potency to the corresponding analogues in **Table 1** (**24** and **25**, respectively) despite the loss of one classic hydrogen bond with Val135 in the hinge region. However, a 10-fold decrease in potency was observed when the phenyl group at the 2-position of the imidazo[1,2-*b*]pyridazine was removed (compare **56** and **57** to **47** and **44**, respectively), due to the loss of hydrophobic contacts that the phenyl group has with neighboring amino acid residues of the protein.

An X-ray co-crystal structure of compound **47** bound in the catalytic site of GSK-3 β was obtained as shown in **Figure 5**. The more potent S-enantiomer of **47** was observed in complex with the protein. Details of the important hydrogen-bonding interactions are shown in **Figure 5A**. A hydrogen bond was observed between the Val135 backbone amide NH of the hinge region and the sp² nitrogen in the six-membered ring of the imidazo[1,2-*b*]pyridazine (2.2 Å), whereas the backbone amide carbonyl oxygen appears to form a potential nonclassic hydrogen-bonding interaction with the aromatic CH in the five-membered ring of the imidazo[1,2-*b*]pyridazine. As was observed with compound **22**, the sp² nitrogen of the pyridine moiety forms a hydrogen bond with the Lys85 amine (1.8 Å), and there was also a water-mediated hydrogen bond between the amide carbonyl and the backbone NH of Asp200. The 2-methylmorpholine group occupies the ribose-binding site and engages in favorable hydrophobic interactions with the protein resulting in an enhancement in potency. An internal hydrogen bond was observed between the amide NH and the N¹ nitrogen of the imidazo[1,2-*b*]pyridazine ring system. A surface representation of the protein with the S-enantiomer of **47** bound to the ATP-binding site of GSK-3 β is shown in **Figure 5B**.

Compounds were tested in a cellular assay wherein the ability of GSK-3 β inhibitors to modulate tau phosphorylation

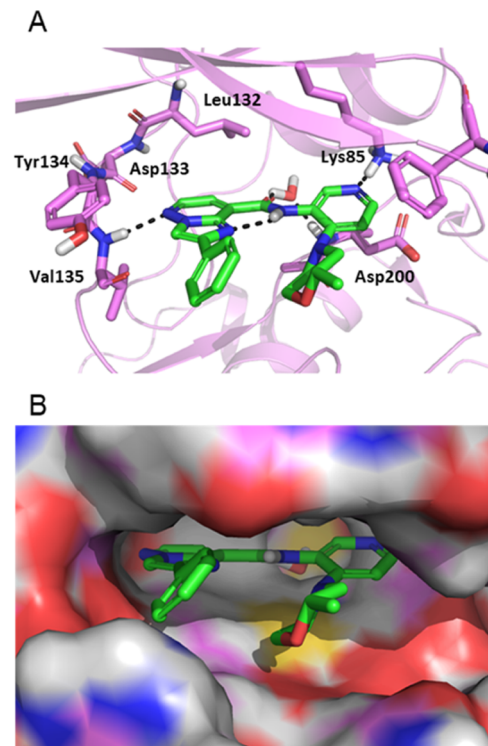


Figure 5. X-ray co-crystal structure of the S-enantiomer of **47** bound in the kinase domain of GSK-3 β (PDB ID: 8DJC) with hydrogens added from a molecular modeling program.⁵⁴ The ATP-binding site is shown. (A) Ligand is rendered as a stick model with green carbon atoms, and hydrogen bonds are shown as black dashed lines. Residues involved in interactions with the ligand are displayed as sticks. The 2-methylmorpholine group occupies the ribose-binding site. (B) Surface representation of the protein with the S-enantiomer of **47** bound to the ATP-binding site of GSK-3 β . Figures are made using PyMOL.⁵⁵

at S396 was measured in a high-content imaging assay in U2OS cells transiently transfected with tau protein. The results for compounds **25**, **38**, **41**, **44**, **45**, **47**, (S)-**47**, (R)-**47**, **48**, **49**, **53**, and **54** are shown in **Table 4**. The pTau IC₅₀ values of the compounds tested in this assay generally followed the same trend observed in the GSK-3 β enzyme assay. Compounds containing either a 4,4-difluoropiperidine or morpholine at R² were among the most potent in the pTau assay (**44**, **45**, and **47**). Compound **41** (R² = Ph) was 15- to 20-fold less potent than analogues with a morpholine group at R² (e.g., **45** and **47**). The potency of **42** in the pTau assay could not be determined, likely due to poor solubility under the assay conditions. Compound (S)-**47** was the most potent compound in this group.

In Vitro Profiling. A subset of compounds was evaluated for kinase selectivity. Broad kinase selectivity screening of compounds was conducted with a panel of 412 kinases (Ambit/DiscoverX/Eurofins).⁶⁰ This is a single-point assay panel with a control for each kinase. Compounds were tested at 1 μ M concentration, and the results are displayed as radial graphs in **Figure 6**. A comparison of the kinase selectivity profiles of compounds **44**, **45**, and **47** indicates that there is a trend toward improved kinase selectivity when comparing **47** to **44** and **45**. The complete Ambit kinase panel heat maps for compounds **44**, **45**, and **47** are included in **Table S2** in the Supporting Information. Kinase selectivity was also assessed in a smaller in-house panel of approximately 30 kinases. GSK-3

Table 4. pTau Inhibitory Activity of Imidazo[1,2-*b*]pyridazine-Based GSK-3 β Inhibitors

cmpd	R ¹	R ²	GSK-3 β IC ₅₀ (nM) ^a	pTau IC ₅₀ (nM) ^b
25	-		0.87 ± 0.44	41 ± 3 ^a
38	Ph	O <i>i</i> Pr	0.70 ± 0.08	83 ± 24
41	Ph	Ph	3.6 ± 0.7	910 ± 300
44	Ph		0.37 ± 0.04	30 ± 5
45	Ph		0.42 ± 0.01	36 ± 16
47	Ph		0.73 ± 0.27 ^b	58 ± 21
(S)-47	Ph		0.13 ± 0.03 ^b	9.2 ± 2.4
(R)-47	Ph		0.82 ± 0.16	86 ± 43
48	2-OMe-Ph		0.57 ± 0.26	58 ± 26
49	4-CF ₃ -Ph		1.4 ± 0.1	130 ± 20
53	cPr		2.6 ± 0.7	60 ^c
54	cPr		0.43 ± 0.07 ^b	120 ^c

^aValues are means of two determinations. ^bValues are the means of at least three determinations ± SD. ^cValue is the result of a single determination.

and CDKs are members of the CMGC family of kinases, which also includes MAPK and CLK. Compound 47 exhibited more than 1900-fold selectivity against CDK2 ($IC_{50} = 1.4 \mu M$), the closest similar kinase to GSK-3 (overall 33% amino acid identity), and was more than 8700-fold selective against CDKS ($IC_{50} = 6.4 \mu M$). Although 47 showed modest inhibitory activity for AAK1 ($IC_{50} = 0.20 \mu M$), PIM1 ($IC_{50} = 0.38 \mu M$),

and PKC θ ($IC_{50} = 0.36 \mu M$), it nevertheless was at least 270-fold selective for GSK-3 β against these kinases. The IC_{50} value of 47 against all of the other off-target kinases in the in-house panel was $>2.0 \mu M$.⁶¹

Additional in vitro profiling data for compounds 41, 42, 44, 45, 47, and 53 are shown in Table 5. Assessment of metabolic stability by incubation of the test compounds for 10 min with human and mouse liver microsomes indicated that 41 and 42 have high metabolic stability (>75% of parent compound remaining after 10 min), whereas 44, 45, 47, and 53 have low metabolic stability (<50% of parent compound remaining after 10 min). A metabolite ID study with 47 indicated that the major soft spot in both human and mouse liver microsomes was the pyridine-2-methylmorpholine moiety, which was subject to oxidation and bis-oxidation. The 2-methylmorpholine ring itself was also subject to oxidation and ring opening as well as dehydrogenation. Glutathione (GSH) conjugation was not observed. It is important to note, however, that the results obtained in the in vitro metabolic stability assay were not necessarily predictive of the in vivo disposition of compounds in this chemotype in mouse pharmacokinetic studies (see below). In general, compounds in this chemotype exhibited high plasma protein binding. Compounds 41, 42, and 44 were particularly highly protein bound with plasma-free fractions of only 0.2–0.3% in mouse. Compounds 45 and 47 had several-fold higher unbound fractions in mouse plasma relative to 44, although the plasma protein binding for these compounds was still quite high. Replacement of the phenyl group in 47 with a cyclopropyl group (53) resulted in an additional increase in the unbound fraction, which can be attributed to the reduced lipophilicity of this compound. The plasma-free fraction for 53 was 1.5 and 3.1% for human and mouse, respectively. The parallel artificial membrane permeability assay (PAMPA) was used to measure passive permeability across membranes. The results shown in Table 5 indicate that these compounds are highly permeable. Permeability was also measured in Caco-2 cells, which have transporter proteins and efflux proteins present. Compounds 45, 47, and 53 exhibited high permeability across Caco-2 cells and 44 was also permeable, although somewhat less so than the former three compounds. These compounds were not P-glycoprotein (P-gp) substrates as indicated by the B-A/A-B ratio (<1) (Table 5). The cLog P values for the compounds in Table 5 range from 1.6 to 3.5,⁶² and the tPSA for this group of compounds varies from 72 to 85 Å²,⁶³ a desirable range for blood–brain barrier penetration. Compounds 45, 47, and 53 have calculated ligand efficiency (LE) values of 0.43, 0.40, and 0.42, respectively, and calculated lipophilic ligand efficiency (LLE) values of 6.88, 6.14, and 6.98, respectively.⁶⁴ The aqueous solubility of 47 at pH 1 and pH 7.4 and in fasted state simulated intestinal fluid (FaSSIF) (pH 6.5) and fed state simulated intestinal fluid (FeSSIF) (pH 5) was 1.22, 0.014, 0.021, and 0.788 mg/mL, respectively.⁶⁵

Pharmacokinetic Studies. To understand the in vivo disposition of compounds 45, 47, and 53, pharmacokinetic studies were conducted in male C57BL6 mice, and the results are shown in Table 6. When dosed intravenously at 2 mg/kg, compounds 45 and 47 exhibited low clearance (10.6 and 3.8 mL min⁻¹ kg⁻¹, respectively). Compound 45 had a half-life of 3.1 h, whereas 47 had a longer half-life of 5.2 h. Volume of distribution (V_{ss}) exceeded total body water volume for 45 and 47. When administered orally as a solution at a dose of 10 mg/kg, compounds 45 and 47 were well absorbed and both

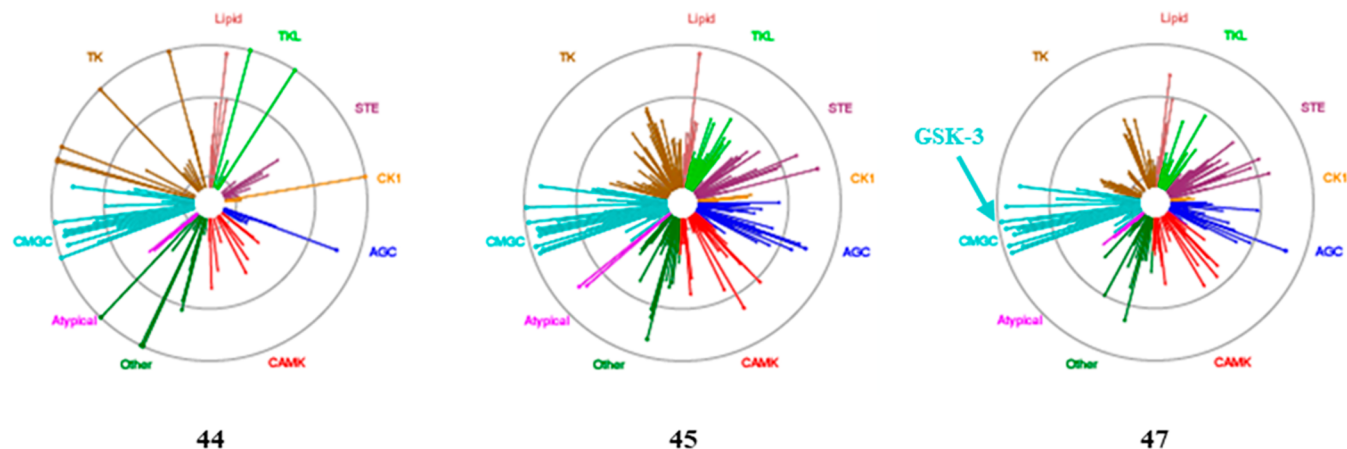


Figure 6. Ambit radial graphs for compounds **44**, **45**, and **47**. Each line represents the remaining activity of a single kinase in the presence of 1 μ M test compound. Individual kinases are grouped into families represented by differing line colors. Starting from the center, the circles indicate 83, 33, and 0% of control binding remaining. SI33 is the percentage of kinases that had $\leq 33\%$ of control binding remaining in the presence of 1 μ M test compound. SI33 = 5.3, 5.8, and 4.1 for **44**, **45**, and **47**, respectively.

Table 5. In Vitro Profiling Data for Compounds 41, 42, 44, 45, 47, and 53

cmpd	metabolic stability (H/M) ^a	plasma protein binding (% unbound, H/M)	PAMPA P_e pH 5.5/7.4 (10^{-6} cm/s)	Caco-2 P_e A-B/B-A (10^{-6} cm/s)	cLog P	tPSA (\AA^2)
41	79/83	<0.1/0.3	20.2/28.2	ND	3.4	72
42	91/92	0.3/0.2	96/ND	ND	3.5	72
44	40/36	0.5/0.2	58.1/64.2	7.0/3.0	3.3	75
45	31/9	1.2/1.0	7.8/29.8	32.2/9.9	2.5	85
47	17/7	0.8/0.9	100/80.6	13.8/7.1	3.0	85
53	3/4	1.5/3.1	86.9/107	22.3/13.3	1.6	85

^aMetabolic stability in human (H) and mouse (M) liver microsomes; values are percentage of parent remaining after 10 min of incubation. ND = not determined.

Table 6. Pharmacokinetic Parameters of Compounds 45, 47, and 53 in Mice

cmpd	IV PK parameters ^a				Oral PK parameters ^b		
	CL ($\text{mL min}^{-1} \text{kg}^{-1}$)	V_{ss} (L/kg)	MRT (h)	$t_{1/2}$ (h)	AUC _{tot} ($\mu\text{M}\cdot\text{h}$)	C_{max} (μM)	F%
45	10.6	1.5	2.4	3.1	47.0	10.7	~100
47	3.8	1.1	4.8	5.2	68.3	7.8	64
53	49.5	1.9	0.6	1.1	3.3	1.3	37

^aIV dose 2 mg/kg, vehicle: 40% poly(ethylene glycol) (PEG) 400/35% 50 mM citrate (pH 4)/15% hydroxypropyl β cyclodextrin (HP- β -CD)/10% dimethyl acetamide (DMAC), ($n = 3$). ^bPO dose 10 mg/kg, vehicle: 83.3% PEG 400/14.7% 50 mM citrate (pH 4)/2% Povidone (PVP)-K30, ($n = 3$).

compounds showed high oral bioavailability ($F\% = \sim 100$ and 64%, respectively). The pharmacokinetic profile of **47** along with the concentration at each time point is included in the Supporting Information (Figure S1). When dosed intravenously, compound **53** exhibited moderate clearance ($49.5 \text{ mL min}^{-1} \text{ kg}^{-1}$) and a short half-life of 1.1 h. When **53** was dosed orally, the exposure was lower than that observed for **45** and **47** and the oral bioavailability was 37%. The disconnect between the in vitro metabolic stability and in vivo pharmacokinetic profiles of compounds **45**, **47**, and **53** can likely be attributed to the high plasma protein binding of these compounds. While it is well appreciated that a higher rate of intrinsic clearance leads to higher clearance in vivo, the extent of plasma protein binding also plays a significant role in the clearance of compounds in vivo and can alter the pharmacokinetic profile relative to what might be anticipated on the basis of the in vitro metabolic stability results alone.^{66,67} Poor aqueous solubility precluded evaluation of **41**, **42**, and **44** in mouse in vivo studies.

Inhibition of Tau Phosphorylation. Compound **47** was evaluated in a triple-transgenic mouse Alzheimer's disease model using LaFerla 3xTg-C57BL6 mice.⁶⁸ Of the above three compounds, **47** had the lowest rate of clearance in the mouse pharmacokinetic study. LaFerla 3xTg-C57BL6 mice have elevated levels of hyperphosphorylated tau (pTau) protein and progressively develop plaques and tangles that are hallmarks of Alzheimer's disease. Lithium chloride was used as a positive control at a dose of 250 mg/kg (ip). In this experiment, oral administration of **47** as a solution at a dose of 30 mg/kg ($n = 6$) resulted in a 52% reduction in pTau396. The effect was comparable to the level of reduction observed with lithium chloride. The results are shown in Figure 7. pTau levels shown are normalized to total Tau. The maximum pTau reduction that can be achieved with GSK-3 inhibition in this model is $\sim 50\%$, which is likely due to the action of other kinases.⁵⁰ Terminal plasma and brain exposures were measured at the conclusion of the experiment (5 h), and it was found that **47** had an exposure of $3.8 \pm 0.8 \mu\text{M}$ in plasma and $1.3 \pm$

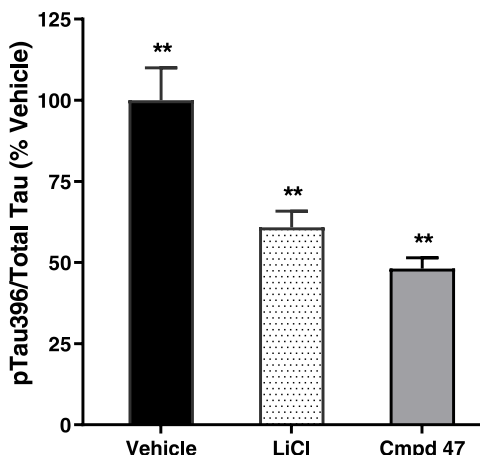


Figure 7. In vivo results in the triple-transgenic mouse Alzheimer's disease model. Oral administration of compound 47 resulted in a 52% reduction in pTau396 when dosed at 30 mg/kg as a solution [83.4% PEG 400/14.7% 50 mM citrate (pH 3)/2% PVP-K30] in LaFerla 3xTg-C57BL6 mice ($n = 6$). Lithium chloride was dosed orally at 250 mg/kg (ip) as a positive control. Results were obtained at 5 h post dose. Data were analyzed by analysis of variance (ANOVA) followed by Dunnett's post hoc test, ** $P < 0.01$ compared to vehicle.

0.4 μ M in brain, resulting in a brain-to-plasma (B/P) ratio of 0.34. The unbound fraction of 47 in mouse brain tissue homogenate ($f_{u,b}$) was measured and was determined to be 0.9%, which was equivalent to the unbound fraction in mouse plasma, resulting in an unbound brain-to-unbound plasma ratio ($K_{p,uu}$) of 0.34.

CONCLUSIONS

In summary, inhibition of GSK-3 β is a potential approach for the treatment of Alzheimer's disease. This report describes the discovery of a new class of imidazo[1,2-*b*]pyridazine-based GSK-3 β inhibitors. Highly potent analogues with subnanomolar GSK-3 β enzyme inhibitor potency were identified. SAR studies combined with X-ray co-crystal structure results showed that only one classic hydrogen-bonding interaction with Val135 in the hinge-binding region of the kinase is necessary to achieve excellent GSK-3 β potency with this chemotype. In the X-ray co-crystal structures, an internal hydrogen bond was observed between the amide NH and the N^1 nitrogen of the imidazo[1,2-*b*]pyridazine ring system. This internal hydrogen bond along with favorable dipole interactions predispose the amide to favor the bioactive conformation. Compounds in this chemotype showed high permeability in the PAMPA and Caco-2 assays. Screening of selected compounds in an Ambit panel containing 412 kinases and in an in-house panel of approximately 30 kinases indicated that good overall kinase selectivity was achieved with excellent selectivity against CDK2. Compound 47 was evaluated in vivo, and it was found that this compound showed high oral bioavailability in a mouse pharmacokinetic study and significantly reduced tau phosphorylation in a triple-transgenic mouse Alzheimer's disease model. Measurement of the plasma and brain levels of 47 revealed that this compound is a moderately brain-penetrant GSK-3 β inhibitor. The encouraging results described herein provide the basis for further optimization of the physicochemical and pharmacokinetic properties of compounds in this class of GSK-3 β inhibitors.

EXPERIMENTAL SECTION

General Chemistry Details. All procedures were carried out under a nitrogen atmosphere unless otherwise indicated using anhydrous solvents purchased from commercial sources without further purification. Reactions requiring anhydrous conditions were performed in glassware, which was oven-dried and placed under a nitrogen atmosphere. Normal phase column chromatography was performed on silica gel using a Biotage system and the solvent systems indicated. Solvent systems are reported as v/v percent ratios. Reversed-phase chromatography was performed using preparative high-performance liquid chromatography (HPLC) instruments (Varian or Shimadzu). All reactions were monitored by thin-layer chromatography (TLC) using EM Science, 0.25 mm, precoated silica gel plates or by liquid chromatography/mass spectrometer (LC/MS). TLC plates were visualized by UV light or staining agents (Hanessian's stain or KMnO₄ stain). For LC/MS monitoring, samples were run on a Shimadzu Nexera series ultraperformance liquid chromatography (UPLC) with a single quadrupole LCMS-2020 mass spectrometer. Yields refer to chromatographically and spectroscopically pure compounds, except as otherwise indicated. Proton (¹H NMR), carbon (¹³C NMR), and fluorine (¹⁹F) nuclear magnetic resonance spectra were recorded on either a Bruker 400 or 500 MHz NMR spectrometer and were obtained in CDCl₃, CD₃OD, or DMSO-*d*₆. The following abbreviations were utilized to describe peak patterns when appropriate: br = broad, s = singlet, d = doublet, t = triplet, q = quartet, m = multiplet, dd = doublet of doublet, dt = doublet of triplets, td = triplet of doublets, and tt = triplet of triplets. Chemical shifts are reported in ppm relative to either the reference solvent of the sample in which they were run or tetramethylsilane (TMS). Coupling constants (*J*) are reported in Hz. Low-resolution mass spectra were obtained from a Shimadzu Nexera series UPLC with a single quadrupole LCMS-2020 mass spectrometer using an electrospray ionization (ESI) method which was operated in positive ionization mode. High-resolution mass spectra (HRMS) were obtained from a Waters Acquity UPLC system equipped with a Thermo Fisher QExactive mass spectrometer using an electrospray ionization (ESI) method which was operated in positive ionization mode. The purity of final products was determined by HPLC. All final products had a purity of $\geq 95\%$ unless noted otherwise.

Analytical HPLC Methods. The following analytical HPLC methods were used for determining the purity of final products.

Analytical HPLC Method A. Column: Waters Sunfire C18 (4.6 mm \times 150 mm, 3.5 μ m); mobile phase A: H₂O with 0.1% TFA; mobile phase B: MeCN with 0.1% TFA; gradient: 10–95% B over 15 min, hold at 95% B for 5 min; flow rate: 1 mL/min; detector wavelength: 254 nm.

Analytical HPLC Method B. Column: Waters XBridge Phenyl (4.6 mm \times 150 mm, 3.5 μ m); mobile phase A: H₂O with 0.1% TFA; mobile phase B: MeCN with 0.1% TFA; gradient: 10–95% B over 15 min, hold at 95% B for 5 min; flow rate: 1 mL/min; detector wavelength: 254 nm.

Analytical HPLC Method C. Column: Waters XTERRA C18 (4.6 mm \times 30 mm, 3.5 μ m); mobile phase A: 10% MeOH/90% H₂O with 0.1% TFA; mobile phase B: 90% MeOH/10% H₂O with 0.1% TFA; gradient: 0–100% B over 12 min, hold at 100% B for 10 min; flow rate: 1 mL/min; detector wavelength: 254 nm.

Analytical HPLC Method D. Column: Phenomenex LUNA Phenyl-Hex (4.6 mm \times 150 mm, 3.5 μ m); mobile phase A: 10% MeOH/90% H₂O with 0.1% TFA; mobile phase B: 90% MeOH/10% H₂O with 0.1% TFA; gradient: 0–100% B over 12 min, hold at 100% B for 10 min; flow rate: 1 mL/min; detector wavelength: 254 nm.

Analytical HPLC Method E. Column: Waters Aquity UPLC BEH C18 (2.1 mm \times 50 mm, 1.7 μ m); mobile phase A: 5% MeCN/95% H₂O with 0.05% TFA; mobile phase B: 95% MeCN/5% H₂O with 0.05% TFA; gradient: 0–100% B over 3.0 min, hold at 100% B for 0.5 min; flow rate: 1 mL/min; detector wavelength: 220 nm; temperature: 50 °C.

Analytical HPLC Method F. Column: Waters Acquity UPLC BEH Phenyl (2.1 mm \times 50 mm, 1.7 μ m); mobile phase A: 5% MeCN/95%

H_2O with 0.05% TFA; mobile phase B: 95% MeCN/5% H_2O with 0.05% TFA; gradient: 0–100% B over 3.0 min, hold at 100% B for 0.5 min; flow rate: 1 mL/min; detector wavelength: 220 nm; temperature: 50 °C.

Preparative HPLC Methods. The following preparative HPLC method was used for the purification of final products.

Preparative HPLC Method A. Column: Waters Sunfire C18 (30 mm × 150 mm, 5 μm); mobile phase A: 5% MeCN/95% H_2O with 0.1% TFA; mobile phase B: 95% MeCN/5% H_2O with 0.1% TFA; gradient: 10–100% B over 20 min, hold at 100% B for 5 min; flow rate: 40 mL/min; detector wavelength: 254 nm.

Ethyl 3,6-Dichloropyridazine-4-carboxylate (11). To a mixture of 3,6-dichloropyridazine-4-carboxylic acid (10) (15.0 g, 78 mmol) in THF (150 mL) were added EtOH (18.2 mL, 311 mmol) and DMAP (0.950 g, 7.77 mmol). EDC (16.4 g, 85 mmol) was added in portions over 1 min. The reaction was mildly exothermic. The reaction mixture was stirred at 22 °C for 16 h. The mixture was transferred to a separatory funnel containing saturated aqueous NaHCO_3 (150 mL). The aqueous layer was extracted with Et_2O (3 × 250 mL). The combined organic layers were washed with brine (100 mL), dried over MgSO_4 , filtered, and concentrated under vacuum. The product was purified by column chromatography on silica gel (20–40% EtOAc in hexanes) to afford 11 (13.2 g, 59.7 mmol, 77% yield) as a colorless oil. ^1H NMR (400 MHz, CDCl_3) δ 7.88 (s, 1H), 4.50 (q, J = 7.0 Hz, 2H), 1.46 (t, J = 7.2 Hz, 3H). MS (ESI) m/z : 221.1 ($\text{M} + \text{H}$)⁺.

Ethyl 6-Chloro-3-((4-methoxybenzyl)amino)pyridazine-4-carboxylate (12). A mixture of ethyl 3,6-dichloropyridazine-4-carboxylate (11) (2.00 g, 9.05 mmol), (4-methoxyphenyl)methanamine (1.24 g, 9.05 mmol), and DIPEA (4.74 mL, 27.1 mmol) in 1,4-dioxane (20 mL) in a sealed vessel was stirred at 80 °C for 20 min. The mixture was concentrated under vacuum, and the product was purified by column chromatography on silica gel (20–30% EtOAc in hexanes) to afford 12 (2.50 g, 7.77 mmol, 86% yield) as a green solid. ^1H NMR (400 MHz, CDCl_3) δ 7.86 (br s, 1H), 7.76 (s, 1H), 7.36 (d, J = 8.8 Hz, 2H), 6.90 (d, J = 8.8 Hz, 2H), 4.80 (d, J = 5.3 Hz, 2H), 4.39 (q, J = 7.1 Hz, 2H), 3.82 (s, 3H), 1.41 (t, J = 7.0 Hz, 3H). MS (ESI) m/z : 322.1 ($\text{M} + \text{H}$)⁺.

Ethyl 3-Amino-6-chloropyridazine-4-carboxylate (13). A mixture of ethyl 6-chloro-3-((4-methoxybenzyl)amino)pyridazine-4-carboxylate (12) (2.50 g, 7.77 mmol) and TFA (12.0 mL, 155 mmol) was heated at reflux for 3 h. The reaction mixture was concentrated under vacuum and transferred to a separatory funnel containing saturated aqueous NaHCO_3 (15 mL). The aqueous layer was extracted with EtOAc (3 × 20 mL). The combined organic layers were washed with brine (15 mL), dried over MgSO_4 , filtered, and concentrated under vacuum. The product was purified by column chromatography on silica gel (60–80% EtOAc in hexanes) to afford 13 (1.00 g, 4.96 mmol, 64% yield) as a green solid. ^1H NMR (400 MHz, CDCl_3) δ 7.77 (s, 1H), 7.00 (br s, 2H), 4.40 (q, J = 7.0 Hz, 2H), 1.40 (t, J = 7.2 Hz, 3H). MS (ESI) m/z : 202.0 ($\text{M} + \text{H}$)⁺.

Ethyl 6-Chloroimidazo[1,2-b]pyridazine-8-carboxylate (14). Chloroacetaldehyde (50% in H_2O) (5.04 mL, 39.7 mmol) was added to ethyl 3-amino-6-chloropyridazine-4-carboxylate (13) (1.00 g, 4.96 mmol) in isopropanol (20 mL). The solution was stirred at 80 °C for 4 h. The mixture was concentrated under vacuum to remove the isopropanol. The resultant orange liquid was partitioned between Et_2O (30 mL) and saturated aqueous NaHCO_3 (20 mL). The organic layer was washed with H_2O (20 mL) and brine (20 mL), dried over MgSO_4 , filtered, and concentrated under vacuum. The product was purified by column chromatography on silica gel (60–80% EtOAc in hexanes) to afford 14 (750 mg, 3.32 mmol, 67% yield) as a green solid. ^1H NMR (400 MHz, CDCl_3) δ 8.04 (d, J = 1.2 Hz, 1H), 7.95 (d, J = 1.1 Hz, 1H), 7.63 (s, 1H), 4.58 (q, J = 7.1 Hz, 2H), 1.49 (t, J = 7.1 Hz, 3H). MS (ESI) m/z : 226.0 ($\text{M} + \text{H}$)⁺.

Ethyl 6-Chloro-3-nitroimidazo[1,2-b]pyridazine-8-carboxylate (15). A 50 mL round-bottom flask was charged with ethyl 6-chloroimidazo[1,2-b]pyridazine-8-carboxylate (14) (600 mg, 2.66 mmol) and was cooled to 0 °C. H_2SO_4 (3 mL, 56.3 mmol) was added to the flask followed by the slow addition of fuming HNO_3 (3.57 mL,

80 mmol). The mixture was stirred at 0 °C for 30 min and then at 22 °C for 5 h. The mixture was neutralized with saturated aqueous Na_2CO_3 solution. The mixture was transferred to a separatory funnel and was extracted with EtOAc (3 × 50 mL). The combined organic layers were washed with brine (50 mL), dried over MgSO_4 , filtered, and concentrated under vacuum to afford 15 (480 mg, 1.77 mmol, 67% yield) as a yellow solid. ^1H NMR (400 MHz, CD_3OD) δ 8.74 (s, 1H), 8.12 (s, 1H), 4.55 (q, J = 7.1 Hz, 2H), 1.46 (t, J = 7.2 Hz, 3H). MS (ESI) m/z : 271.0 ($\text{M} + \text{H}$)⁺.

Ethyl 3-Aminoimidazo[1,2-b]pyridazine-8-carboxylate (16). A mixture of ethyl 6-chloro-3-nitroimidazo[1,2-b]pyridazine-8-carboxylate (15) (480 mg, 1.77 mmol), 10% palladium on carbon (378 mg, 0.355 mmol), and TEA (0.494 mL, 3.55 mmol) in EtOH (10 mL) and DMF (10 mL) was placed under H_2 at 3 atm (45 psi) for 4 h. The catalyst was removed by filtration and the filtrate was concentrated under vacuum. The product was purified by column chromatography on silica gel (10% MeOH in CH_2Cl_2) to afford 16 (300 mg, 1.46 mmol, 82% yield) as a dark red oil. ^1H NMR (400 MHz, CD_3OD) δ 8.52 (d, J = 4.8 Hz, 1H), 7.44 (d, J = 4.8 Hz, 1H), 7.24 (s, 1H), 4.50 (q, J = 7.0 Hz, 2H), 1.44 (t, J = 7.2 Hz, 3H). MS (ESI) m/z : 207.1 ($\text{M} + \text{H}$)⁺.

Ethyl 3-((Cyclopropylmethyl)amino)imidazo[1,2-b]pyridazine-8-carboxylate (17). To a solution of ethyl 3-aminoimidazo[1,2-b]pyridazine-8-carboxylate (16) (150 mg, 0.727 mmol) and acetic acid (0.083 mL, 1.46 mmol) in MeOH (5 mL) was added cyclopropanecarboxaldehyde (0.055 mL, 0.727 mmol). The mixture was stirred at 22 °C for 1 h. NaBH_3CN (91 mg, 1.46 mmol) was added and the mixture was stirred at 22 °C for 2 h. The mixture was concentrated under vacuum, and the product was purified by column chromatography on silica gel (30–80% EtOAc in hexanes) to afford 17 (95 mg, 0.365 mmol, 50% yield) as a red solid. ^1H NMR (400 MHz, CDCl_3) δ 8.35 (d, J = 4.8 Hz, 1H), 7.36 (d, J = 4.8 Hz, 1H), 7.29 (s, 1H), 4.55 (q, J = 7.0 Hz, 2H), 3.19 (d, J = 7.0 Hz, 2H), 1.46 (t, J = 7.2 Hz, 3H), 1.28–1.12 (m, 1H), 0.64–0.56 (m, 2H), 0.34–0.28 (m, 2H). MS (ESI) m/z : 261.2 ($\text{M} + \text{H}$)⁺.

3-(Cyclopropylmethyl)amino)imidazo[1,2-b]pyridazine-8-carboxylic Acid (18). A mixture of ethyl 3-((cyclopropylmethyl)amino)imidazo[1,2-b]pyridazine-8-carboxylate (17) (110 mg, 0.423 mmol) and LiOH· H_2O (70.9 mg, 1.69 mmol) in H_2O (0.2 mL) and THF (5 mL) was stirred at 22 °C for 2 h. The mixture was concentrated under vacuum to afford 18 (180 mg, 0.388 mmol, 92% yield) as a red solid. The crude product was used directly in the next step. MS (ESI) m/z : 233.1 ($\text{M} + \text{H}$)⁺.

3-((Cyclopropylmethyl)amino)-N-(pyridin-3-yl)imidazo[1,2-b]pyridazine-8-carboxamide, 2 TFA (19). To a mixture of 3-((cyclopropylmethyl)amino)imidazo[1,2-b]pyridazine-8-carboxylic acid (18) (25 mg, 0.108 mmol), 3-aminopyridine (20.3 mg, 0.215 mmol), and DIPEA (0.056 mL, 0.323 mmol) in DMF (1 mL) was added HATU (61.4 mg, 0.161 mmol). The reaction mixture was stirred at 22 °C for 4 h. The reaction mixture was transferred to a separatory funnel containing saturated aqueous NaHCO_3 (10 mL). The aqueous layer was extracted with CH_2Cl_2 (3 × 10 mL). The combined organic layers were washed with brine (10 mL), dried over MgSO_4 , filtered, and concentrated under vacuum. The product was purified by preparative reversed-phase HPLC (method A) and lyophilized to afford 19 (10 mg, 0.017 mmol, 16% yield) as a red solid. ^1H NMR (400 MHz, $\text{DMSO}-d_6$) δ 11.96 (s, 1H), 8.96 (d, J = 2.3 Hz, 1H), 8.69 (d, J = 4.8 Hz, 1H), 8.42 (dd, J = 4.8, 1.5 Hz, 1H), 8.28–8.25 (m, 1H), 7.56 (d, J = 4.8 Hz, 1H), 7.50 (dd, J = 7.9, 4.6 Hz, 1H), 7.38 (s, 1H), 6.05 (t, J = 6.3 Hz, 1H), 3.17 (t, J = 6.4 Hz, 2H), 1.19 (t, J = 7.0 Hz, 1H), 0.51–0.46 (m, 2H), 0.33–0.29 (m, 2H). MS (ESI) m/z : 309.2 ($\text{M} + \text{H}$)⁺. HPLC purity: >98%, t_{R} = 6.12 min (method A); >98%, t_{R} = 6.50 min (method B).

3-((Cyclopropylmethyl)amino)-N-(4-methylpyridin-3-yl)imidazo[1,2-b]pyridazine-8-carboxamide, 2 TFA (20). Compound 20 was prepared according to the procedure described for the synthesis of 19 using 3-((cyclopropylmethyl)amino)imidazo[1,2-b]pyridazine-8-carboxylic acid (18) (25 mg, 0.108 mmol) and 3-amino-4-methylpyridine (23.3 mg, 0.215 mmol). The product was purified by HPLC (method A) and lyophilized to afford 20 (10 mg, 0.030 mmol, 28%

yield) as a red solid. ^1H NMR (400 MHz, CDCl_3) δ 11.87 (br s, 1H), 9.48 (s, 1H), 8.49 (d, J = 4.5 Hz, 1H), 8.36 (d, J = 5.0 Hz, 1H), 7.75 (d, J = 4.8 Hz, 1H), 7.29 (s, 1H), 7.22 (d, J = 5.0 Hz, 1H), 7.18 (s, 1H), 3.22 (t, J = 6.5 Hz, 2H), 2.55 (s, 3H), 1.29–1.20 (m, 1H), 0.69–0.62 (m, 2H), 0.38–0.31 (m, 2H). HRMS (ESI) m/z : 323.1615 [(M + H) $^+$, calcd for $\text{C}_{17}\text{H}_{19}\text{N}_6\text{O}$ 323.1620]. HPLC purity: 96%, t_{R} = 7.47 min (method A); 96%, t_{R} = 8.06 min (method B).

3-((Cyclopropylmethyl)amino)-N-(4-isopropoxypyridin-3-yl)-imidazo[1,2-b]pyridazine-8-carboxamide, 2 TFA (21). Compound 21 was prepared according to the procedure described for the synthesis of 19 using 3-((cyclopropylmethyl)amino)imidazo[1,2-b]pyridazine-8-carboxylic acid (18) (20 mg, 0.086 mmol) and 4-isopropoxypyridin-3-amine, HCl (38.8 mg, 0.172 mmol). The product was purified by preparative reversed-phase HPLC (method A) and lyophilized to afford 21 (24 mg, 0.040 mmol, 46% yield) as a red solid. ^1H NMR (400 MHz, $\text{DMSO}-d_6$) δ 12.82 (s, 1H), 9.71 (s, 1H), 8.71 (d, J = 4.5 Hz, 1H), 8.68 (d, J = 6.5 Hz, 1H), 7.81 (d, J = 6.3 Hz, 1H), 7.62 (d, J = 4.5 Hz, 1H), 7.38 (s, 1H), 5.25 (dt, J = 12.0, 5.9 Hz, 1H), 3.18 (d, J = 6.8 Hz, 2H), 1.57 (d, J = 6.0 Hz, 6H), 1.25–1.13 (m, 1H), 0.52–0.46 (m, 2H), 0.34–0.28 (m, 2H). HRMS (ESI) m/z : 367.1875 [(M + H) $^+$, calcd for $\text{C}_{19}\text{H}_{23}\text{N}_6\text{O}_2$ 367.1882]. HPLC purity: 100%, t_{R} = 9.52 min (method A); 100%, t_{R} = 9.90 min (method B).

3-((Cyclopropylmethyl)amino)-N-(4-phenylpyridin-3-yl)-imidazo[1,2-b]pyridazine-8-carboxamide, 2 TFA (22). Compound 22 was prepared according to the procedure described for the synthesis of 19 using 3-((cyclopropylmethyl)amino)imidazo[1,2-b]pyridazine-8-carboxylic acid (18) (20 mg, 0.086 mmol) and 4-phenylpyridin-3-amine, HCl (41.9 mg, 0.172 mmol). The product was purified by preparative reversed-phase HPLC (method A) and lyophilized to afford 22 (15 mg, 0.023 mmol, 27% yield) as a red solid. ^1H NMR (400 MHz, $\text{DMSO}-d_6$) δ 11.87 (s, 1H), 9.59 (s, 1H), 8.65 (d, J = 4.8 Hz, 1H), 8.56 (d, J = 5.0 Hz, 1H), 7.63–7.48 (m, 8H), 6.87 (s, 1H), 3.09 (d, J = 6.8 Hz, 2H), 0.90–0.81 (m, 1H), 0.53–0.40 (m, 2H), 0.32–0.22 (m, 2H). HRMS (ESI) m/z : 385.1768 [(M + H) $^+$, calcd for $\text{C}_{22}\text{H}_{21}\text{N}_6\text{O}$ 385.1777]. HPLC purity: 98.6%, t_{R} = 9.76 min (method A); 98.5%, t_{R} = 10.16 min (method B).

3-((Cyclopropylmethyl)amino)-N-(4-morpholinopyridin-3-yl)-imidazo[1,2-b]pyridazine-8-carboxamide, 2 TFA (23). Compound 23 was prepared according to the procedure described for the synthesis of 19 using 3-((cyclopropylmethyl)amino)imidazo[1,2-b]pyridazine-8-carboxylic acid (18) (30 mg, 0.129 mmol) and 4-morpholinopyridin-3-amine (46.3 mg, 0.258 mmol). The product was purified by preparative reversed-phase HPLC (method A) and lyophilized to afford 23 (28 mg, 0.043 mmol, 33% yield) as a red oil. ^1H NMR (400 MHz, $\text{DMSO}-d_6$) δ 12.01 (s, 1H), 9.34 (s, 1H), 8.72 (d, J = 4.5 Hz, 1H), 8.49 (d, J = 5.8 Hz, 1H), 7.62 (d, J = 4.5 Hz, 1H), 7.51 (d, J = 6.5 Hz, 1H), 7.47 (s, 1H), 3.91–3.81 (m, 4H), 3.40 (br s, 4H), 3.18 (d, J = 6.8 Hz, 2H), 1.22–1.12 (m, 1H), 0.54–0.43 (m, 2H), 0.35–0.25 (m, 2H). HRMS (ESI) m/z : 394.1986 [(M + H) $^+$, calcd for $\text{C}_{20}\text{H}_{24}\text{N}_7\text{O}_2$ 394.1991]. HPLC purity: 97%, t_{R} = 7.69 min (method A); 94%, t_{R} = 7.93 min (method B).

3-((Cyclopropylmethyl)amino)-N-(4-(2-methylmorpholino)pyridin-3-yl)-imidazo[1,2-b]pyridazine-8-carboxamide, 2 TFA (24). Compound 24 was prepared according to the procedure described for the synthesis of 19 using 3-((cyclopropylmethyl)amino)imidazo[1,2-b]pyridazine-8-carboxylic acid (18) (30 mg, 0.129 mmol) and 4-(2-methylmorpholino)pyridin-3-amine (49.9 mg, 0.258 mmol). The product was purified by preparative reversed-phase HPLC (method A) and lyophilized to afford 24 (29 mg, 0.043 mmol, 34% yield) as a red oil. ^1H NMR (400 MHz, $\text{DMSO}-d_6$) δ 11.95 (s, 1H), 9.28 (s, 1H), 8.72 (d, J = 4.8 Hz, 1H), 8.53–8.46 (m, 1H), 7.61 (d, J = 4.5 Hz, 1H), 7.55 (d, J = 6.8 Hz, 1H), 7.45 (s, 1H), 3.94–3.70 (m, 7H), 3.18 (d, J = 6.8 Hz, 2H), 1.23–1.15 (m, 1H), 1.07 (d, J = 6.3 Hz, 3H), 0.53–0.45 (m, 2H), 0.35–0.27 (m, 2H). HRMS (ESI) m/z : 408.2142 [(M + H) $^+$, calcd for $\text{C}_{21}\text{H}_{26}\text{N}_7\text{O}_2$ 408.2148]. HPLC purity: 98.5%, t_{R} = 8.50 min (method A); 95.6%, t_{R} = 8.35 min (method B).

3-((Cyclopropylmethyl)amino)-N-(4-(4,4-difluoropiperidin-1-yl)pyridin-3-yl)-imidazo[1,2-b]pyridazine-8-carboxamide, 2 TFA (25). Compound 25 was prepared according to the procedure described for

the synthesis of 19 using 3-((cyclopropylmethyl)amino)imidazo[1,2-b]pyridazine-8-carboxylic acid (18) (30 mg, 0.129 mmol) and 4-(4,4-difluoropiperidin-1-yl)pyridin-3-amine (55.1 mg, 0.258 mmol). The product was purified by preparative reversed-phase HPLC (method A) and lyophilized to afford 25 (26 mg, 0.039 mmol, 30% yield) as a red oil. ^1H NMR (400 MHz, $\text{DMSO}-d_6$) δ 12.00 (s, 1H), 9.34 (s, 1H), 8.79 (d, J = 4.8 Hz, 1H), 8.73 (d, J = 4.8 Hz, 1H), 8.52 (d, J = 6.5 Hz, 1H), 7.64 (d, J = 4.8 Hz, 1H), 7.62 (d, J = 6.5 Hz, 1H), 7.35 (s, 1H), 3.53–3.48 (m, 4H), 3.17 (d, J = 6.8 Hz, 2H), 2.32–2.18 (m, 4H), 1.22–1.13 (m, 1H), 0.52–0.45 (m, 2H), 0.33–0.28 (m, 2H). MS (ESI) m/z : 428.2 (M + H) $^+$. HPLC purity: 100%, t_{R} = 9.10 min (method A); 100%, t_{R} = 9.50 min (method B).

Ethyl 6-Chloro-2-phenylimidazo[1,2-b]pyridazine-8-carboxylate (28a). Ethyl 3-amino-6-chloropyridazine-4-carboxylate (13) (600 mg, 2.98 mmol) was added to a solution of 2-bromoacetophenone (26a) (711 mg, 3.57 mmol) in DMF (10 mL). The solution was stirred at 60 °C for 4 h. The reaction mixture was partitioned between Et_2O (30 mL) and saturated aqueous NaHCO_3 (20 mL). The organic layer was washed with H_2O (20 mL) and brine (20 mL), dried over MgSO_4 , filtered, and concentrated under vacuum. The product was purified by column chromatography on silica gel (5–20% EtOAc in hexanes) to afford 28a (600 mg, 1.99 mmol, 67% yield) as a yellow solid. ^1H NMR (400 MHz, $\text{DMSO}-d_6$) δ 9.08 (s, 1H), 8.12–8.08 (m, 2H), 7.74 (s, 1H), 7.55–7.49 (m, 2H), 7.45–7.40 (m, 1H), 4.49 (q, J = 7.2 Hz, 2H), 1.42 (t, J = 7.0 Hz, 3H). MS (ESI) m/z : 302.0 (M + H) $^+$.

Ethyl 6-Chloro-2-cyclopropylimidazo[1,2-b]pyridazine-8-carboxylate (29). A mixture of ethyl 3-amino-6-chloropyridazine-4-carboxylate (13) (300 mg, 1.49 mmol) and 2-bromo-1-cyclopropylethan-1-one (27) (485 mg, 2.98 mmol) in 1,4-dioxane (5 mL) was stirred at 90 °C for 4 h. The mixture was cooled to 22 °C and was transferred to a separatory funnel containing saturated aqueous NaHCO_3 (20 mL). The aqueous layer was extracted with EtOAc (3 × 20 mL). The combined organic layers were washed with brine (20 mL), dried over MgSO_4 , filtered, and concentrated under vacuum. The product was purified by column chromatography on silica gel (10–60% EtOAc in hexanes) to afford 29 (161 mg, 0.606 mmol, 41% yield) as a yellow solid. ^1H NMR (500 MHz, CDCl_3) δ 7.75 (s, 1H), 7.52 (s, 1H), 4.54 (q, J = 7.2 Hz, 2H), 2.18 (tt, J = 8.3, 5.0 Hz, 1H), 1.48 (t, J = 7.1 Hz, 3H), 1.11–1.06 (m, 2H), 1.03–0.97 (m, 2H). MS m/z : 266.0 (M + H) $^+$.

Ethyl 2-Phenylimidazo[1,2-b]pyridazine-8-carboxylate (30a). A mixture of ethyl 6-chloro-2-phenylimidazo[1,2-b]pyridazine-8-carboxylate (28a) (1.30 g, 4.31 mmol) and 10% palladium on carbon (0.459 g, 0.215 mmol) in CHCl_3 (15 mL) and EtOH (15 mL) was stirred in a 50 mL round-bottom flask under H_2 (1 atm) for 14 h. The catalyst was removed by filtration and the filtrate was concentrated under vacuum. The product was dried under vacuum to afford 30a (500 mg, 43% yield). The product was used directly in the next step. ^1H NMR (400 MHz, CDCl_3) δ 8.43 (d, J = 4.8 Hz, 1H), 8.40 (s, 1H), 8.11–8.07 (m, 2H), 7.61 (d, J = 4.5 Hz, 1H), 7.52–7.46 (m, 2H), 7.43–7.37 (m, 1H), 4.59 (q, J = 7.0 Hz, 2H), 1.54 (t, J = 7.2 Hz, 3H). MS (ESI) m/z : 268.1 (M + H) $^+$.

Ethyl 2-Cyclopropylimidazo[1,2-b]pyridazine-8-carboxylate (31). A mixture of ethyl 6-chloro-2-cyclopropylimidazo[1,2-b]pyridazine-8-carboxylate (29) (146 mg, 0.549 mmol) and 10% palladium on carbon (117 mg, 0.055 mmol) in EtOH (12 mL) was stirred rapidly under H_2 (1 atm) for 20 min. The catalyst was removed by filtration through a pad of Celite, and the filtrate was concentrated under vacuum. The mixture was transferred to a separatory funnel containing H_2O (10 mL). The aqueous layer was extracted with 5% MeOH in CH_2Cl_2 (4 × 15 mL). The combined organic layers were washed with brine (10 mL), dried over MgSO_4 , filtered, and concentrated under vacuum to afford 31 (118 mg, 0.510 mmol, 93% yield) as a yellow oil. The product was used directly in the next step. ^1H NMR (500 MHz, CDCl_3) δ 8.34 (d, J = 4.7 Hz, 1H), 7.79 (s, 1H), 7.51 (d, J = 4.7 Hz, 1H), 4.54 (q, J = 7.1 Hz, 2H), 2.21 (tt, J = 8.4, 5.0 Hz, 1H), 1.48 (t, J = 7.1 Hz, 3H), 1.13–1.05 (m, 2H), 1.03–0.94 (m, 2H). MS m/z : 232.1 (M + H) $^+$.

Ethyl Imidazo[1,2-b]pyridazine-8-carboxylate (32). To a solution of ethyl 6-chloroimidazo[1,2-b]pyridazine-8-carboxylate (14) (170 mg, 0.753 mmol) in EtOH (12 mL) under N₂ was added 10% palladium on carbon (160 mg, 0.075 mmol). The reaction flask was evacuated and placed under H₂. The reaction mixture was stirred rapidly under H₂ (1 atm) for 15 min. The catalyst was removed by filtration, and the filtrate was concentrated under vacuum. The mixture was transferred to a separatory funnel containing H₂O (10 mL). The aqueous layer was extracted with 5% MeOH in CH₂Cl₂ (4 × 15 mL). The combined organic layers were washed with brine (10 mL), dried over MgSO₄, filtered, and concentrated under vacuum to afford 32 (112 mg, 0.586 mmol, 78% yield) as a pale green solid. The product was used directly in the next step. ¹H NMR (500 MHz, CDCl₃) δ 8.46 (d, J = 4.6 Hz, 1H), 8.10 (d, J = 1.1 Hz, 1H), 7.96 (d, J = 1.0 Hz, 1H), 7.63 (d, J = 4.6 Hz, 1H), 4.59 (q, J = 7.1 Hz, 2H), 1.49 (t, J = 7.1 Hz, 3H). MS (ESI) m/z: 192.1 (M + H)⁺.

2-Phenylimidazo[1,2-b]pyridazine-8-carboxylic Acid (33a). A mixture of ethyl 2-phenylimidazo[1,2-b]pyridazine-8-carboxylate (30a) (235 mg, 0.879 mmol) and LiOH·H₂O (111 mg, 2.64 mmol) in H₂O (0.5 mL) and THF (10 mL) was stirred at 22 °C for 2 h. The mixture was concentrated under vacuum to furnish 33a (220 mg, 99% yield), which was used directly in the next step. ¹H NMR (500 MHz, DMSO-d₆) δ 8.84 (s, 1H), 8.58 (d, J = 4.6 Hz, 1H), 8.12–8.06 (m, 2H), 7.55 (d, J = 4.6 Hz, 1H), 7.43–7.38 (m, 2H), 7.37–7.30 (m, 1H). MS (ESI) m/z: 240.1 (M + H)⁺.

2-(2-Methoxyphenyl)imidazo[1,2-b]pyridazine-8-carboxylic Acid (33b). Compound 33b was prepared from ethyl 3-amino-6-chloropyridazine-4-carboxylate (13) (200 mg, 0.992 mmol) and 2-bromo-4'-methoxyacetophenone (26b) (227 mg, 0.992 mmol) following the three-step procedure for the synthesis of 33a from 13. Compound 33b (60 mg, 0.223 mmol) was isolated as a yellow solid. ¹H NMR (400 MHz, CD₃OD) δ 6.95 (s, 1H), 6.86 (d, J = 4.3 Hz, 1H), 6.57 (d, J = 7.0 Hz, 1H), 6.00 (d, J = 4.0 Hz, 1H), 5.72 (t, J = 7.9 Hz, 1H), 5.48 (d, J = 8.3 Hz, 1H), 5.41 (t, J = 7.3 Hz, 1H), 2.36 (s, 3H). MS (ESI) m/z: 270.1 (M + H)⁺.

2-(4-(Trifluoromethyl)phenyl)imidazo[1,2-b]pyridazine-8-carboxylic Acid (33c). Compound 33c was prepared from ethyl 3-amino-6-chloropyridazine-4-carboxylate (13) (270 mg, 1.34 mmol) and 2-bromo-4'-(trifluoromethyl)acetophenone (26c) (358 mg, 1.34 mmol) following the three-step procedure for the synthesis of 33a from 13. Compound 33c (80 mg, 0.260 mmol) was isolated as a yellow solid. ¹H NMR (400 MHz, DMSO-d₆) δ 9.04 (s, 1H), 8.62 (d, J = 4.5 Hz, 1H), 8.35 (br d, J = 8.0 Hz, 2H), 7.80 (br d, J = 8.3 Hz, 2H), 7.58 (d, J = 4.5 Hz, 1H). MS (ESI) m/z: 308.1 (M + H)⁺.

2-Cyclopropylimidazo[1,2-b]pyridazine-8-carboxylic Acid (34). A mixture of ethyl 2-cyclopropylimidazo[1,2-b]pyridazine-8-carboxylate (31) (110 mg, 0.476 mmol) and LiOH·H₂O (59.9 mg, 1.43 mmol) in H₂O (0.15 mL) and THF (3 mL) was stirred at 22 °C for 2 h. The mixture was concentrated under vacuum to afford 34 (112 mg, quantitative yield). The product was used in the next step without further purification. ¹H NMR (400 MHz, DMSO-d₆) δ 8.79 (d, J = 4.8 Hz, 1H), 8.41 (s, 1H), 7.80 (d, J = 4.0 Hz, 1H), 2.27–2.18 (m, 1H), 1.14–1.06 (m, 2H), 0.98–0.92 (m, 2H). MS (ESI) m/z: 204.2 (M + H)⁺.

Imidazo[1,2-b]pyridazine-8-carboxylic Acid (35). To a solution of ethyl imidazo[1,2-b]pyridazine-8-carboxylate (32) (88 mg, 0.460 mmol) in THF (3 mL) at 22 °C was added a solution of LiOH (33.1 mg, 1.38 mmol) in H₂O (0.30 mL). The reaction mixture was stirred at 22 °C for 2 h. The mixture was concentrated under vacuum to furnish 35 (74 mg, 0.454 mmol, 99% yield) as a gray solid. The product was used directly in the next step. ¹H NMR (500 MHz, DMSO-d₆) δ 8.60 (d, J = 4.6 Hz, 1H), 8.32 (d, J = 1.2 Hz, 1H), 7.74 (d, J = 1.1 Hz, 1H), 7.54 (d, J = 4.6 Hz, 1H). ¹³C NMR (126 MHz, DMSO-d₆) δ 163.8, 145.4, 139.2, 135.1, 132.7, 118.8, 117.3. MS (ESI) m/z 164.0 M⁺.

2-Phenyl-N-(pyridin-3-yl)imidazo[1,2-b]pyridazine-8-carboxamide, 2 TFA (36). To a solution of 2-phenylimidazo[1,2-b]pyridazine-8-carboxylic acid (33a) (35 mg, 0.146 mmol) and 3-aminopyridine (6.0 mg, 0.062 mmol) in DMF (1 mL) was added DIPEA (0.036 mL, 0.210 mmol) followed by HATU (32 mg, 0.084 mmol). The reaction

mixture was stirred at 22 °C for 6 h. The mixture was transferred to a separatory funnel containing saturated aqueous NaHCO₃ (15 mL). The aqueous layer was extracted with EtOAc (3 × 15 mL). The combined organic layers were washed with brine (20 mL), dried over MgSO₄, filtered, and concentrated under vacuum. The product was purified by preparative reversed-phase HPLC (method A) and lyophilized to afford 36 (5.5 mg, 0.010 mmol, 42% yield) as a yellow amorphous solid. ¹H NMR (500 MHz, DMSO-d₆) δ 12.11 (s, 1H), 9.15 (s, 1H), 9.08 (d, J = 2.3 Hz, 1H), 8.80 (d, J = 4.6 Hz, 1H), 8.48 (dd, J = 4.7, 1.4 Hz, 1H), 8.41–8.38 (m, 1H), 8.20 (dd, J = 8.3, 1.1 Hz, 2H), 7.88 (d, J = 4.7 Hz, 1H), 7.61–7.54 (m, 3H), 7.47–7.42 (m, 1H). MS (ESI) m/z: 316.1 (M + H)⁺. HPLC purity: 98.1%, t_R = 9.32 min (method A); 98.1%, t_R = 9.56 min (method B).

N-(4-Methylpyridin-3-yl)-2-phenylimidazo[1,2-b]pyridazine-8-carboxamide (37). Compound 37 was prepared according to the procedure described for the synthesis of 36 using 2-phenylimidazo[1,2-b]pyridazine-8-carboxylic acid (33a) (30 mg, 0.125 mmol) and 3-amino-4-methylpyridine (27.1 mg, 0.251 mmol). The product was purified by column chromatography on silica gel (20–60% EtOAc in hexanes) to afford 37 (16 mg, 0.046 mmol, 37% yield) as a yellow solid. ¹H NMR (400 MHz, DMSO-d₆) δ 11.75 (s, 1H), 9.35 (s, 1H), 9.16 (s, 1H), 8.82 (d, J = 4.8 Hz, 1H), 8.35 (d, J = 4.8 Hz, 1H), 8.21–8.11 (m, 2H), 7.94 (d, J = 4.8 Hz, 1H), 7.60–7.51 (m, 2H), 7.48–7.40 (m, 2H), 2.61 (s, 3H). HRMS (ESI) m/z: 330.1344 [(M + H)⁺, calcd for C₁₉H₁₆N₂O 330.1349]. HPLC purity: 98%, t_R = 8.96 min (method A); 98%, t_R = 10.00 min (method B).

N-(4-Isopropoxypyridin-3-yl)-2-phenylimidazo[1,2-b]pyridazine-8-carboxamide (38). Compound 38 was prepared according to the procedure described for the synthesis of 36 using 2-phenylimidazo[1,2-b]pyridazine-8-carboxylic acid (33a) (60 mg, 0.251 mmol) and 4-isopropoxypyridin-3-amine (53.4 mg, 0.351 mmol). The product was purified by column chromatography on silica gel (20% EtOAc with 10% MeOH/80% hexanes–100% EtOAc with 10% MeOH) to afford 38 (42.7 mg, 0.114 mmol, 46% yield) as a yellow solid. ¹H NMR (500 MHz, DMSO-d₆) δ 11.85 (s, 1H), 9.46 (s, 1H), 9.12 (s, 1H), 8.79 (d, J = 4.7 Hz, 1H), 8.32 (d, J = 5.5 Hz, 1H), 8.24–8.17 (m, 2H), 7.92 (d, J = 4.7 Hz, 1H), 7.56–7.50 (m, 2H), 7.49–7.43 (m, 1H), 7.29 (d, J = 5.7 Hz, 1H), 4.93 (dt, J = 12.2, 6.1 Hz, 1H), 1.35 (d, J = 6.1 Hz, 6H). HRMS (ESI) m/z: 374.1605 [(M + H)⁺, calcd for C₂₁H₂₀N₂O₂ 374.1612]. HPLC purity: 98.4%, t_R = 10.13 min (method A); 100%, t_R = 10.62 min (method B).

2-Phenyl-N-(4-(2,2,2-trifluoroethoxy)pyridin-3-yl)imidazo[1,2-b]pyridazine-8-carboxamide (39). Compound 39 was prepared according to the procedure described for the synthesis of 36 using 2-phenylimidazo[1,2-b]pyridazine-8-carboxylic acid (33a) (20 mg, 0.084 mmol) and 4-(2,2,2-trifluoroethoxy)pyridin-3-amine (32.1 mg, 0.167 mmol). The product was purified by column chromatography on silica gel (30–80% EtOAc in hexanes) to afford 39 (15 mg, 0.034 mmol, 41% yield) as a yellow solid. ¹H NMR (400 MHz, DMSO-d₆) δ 11.95 (s, 1H), 9.52 (s, 1H), 9.14 (s, 1H), 8.80 (d, J = 4.8 Hz, 1H), 8.43 (d, J = 5.8 Hz, 1H), 8.17 (d, J = 7.3 Hz, 2H), 7.93 (d, J = 4.8 Hz, 1H), 7.60–7.49 (m, 3H), 7.47–7.38 (m, 1H), 5.21 (q, J = 8.8 Hz, 2H). HRMS (ESI) m/z: 414.1169 [(M + H)⁺, calcd for C₂₀H₁₅F₃N₂O₂ 414.1178]. HPLC purity: >99%, t_R = 10.95 min (method C); >99%, t_R = 11.90 min (method D).

N-(4-(Methylsulfonyl)pyridin-3-yl)-2-phenylimidazo[1,2-b]pyridazine-8-carboxamide (40). To a suspension of 2-phenylimidazo[1,2-b]pyridazine-8-carboxylic acid (33a) (10 mg, 0.042 mmol) in CH₂Cl₂ (1 mL) at 0 °C was added DMF (0.647 μL, 8.36 μmol) and oxalyl chloride (0.011 mL, 0.125 mmol). The mixture was stirred at 22 °C for 1 h. The mixture was concentrated under vacuum. The residue was suspended in CH₂Cl₂ (1 mL) at 0 °C and TEA (0.023 mL, 0.167 mmol), DMAP (10.2 mg, 0.084 mmol), and 4-(methylsulfonyl)pyridin-3-amine (7.9 mg, 0.046 mmol) were added to the mixture. The reaction mixture was stirred at 22 °C for 4 h. The mixture was transferred to a separatory funnel containing saturated aqueous NaHCO₃ (15 mL). The aqueous layer was extracted with CH₂Cl₂ (3 × 15 mL). The combined organic layers were washed with brine (15 mL), dried over MgSO₄, filtered, and concentrated under vacuum. The product was purified by preparative

reversed-phase HPLC (method A) and lyophilized. The product was purified further by preparative thin-layer chromatography (5% MeOH in CH_2Cl_2) to afford **40** (2.0 mg, 5.03 μmol , 12% yield) as a yellow solid. ^1H NMR (400 MHz, CD_3OD) δ 9.53 (s, 1H), 8.76 (s, 1H), 8.74 (d, $J = 5.3$ Hz, 1H), 8.67 (d, $J = 4.8$ Hz, 1H), 8.29 (d, $J = 1.5$ Hz, 1H), 8.27 (s, 1H), 8.06 (d, $J = 5.0$ Hz, 1H), 7.99 (d, $J = 4.5$ Hz, 1H), 7.50–7.43 (m, 3H), 3.29 (s, 3H). MS (ESI) m/z : 394.1 ($\text{M} + \text{H}$) $^+$. HPLC purity: >98%, $t_{\text{R}} = 16.74$ min (method A); >98%, $t_{\text{R}} = 17.89$ min (method B).

2-Phenyl-N-(4-phenylpyridin-3-yl)imidazo[1,2-b]pyridazine-8-carboxamide (41). Compound **41** was prepared according to the procedure described for the synthesis of **36** using 2-phenylimidazo[1,2-b]pyridazine-8-carboxylic acid (**33a**) (50 mg, 0.209 mmol) and 4-phenylpyridin-3-amine (71.1 mg, 0.418 mmol). The product was purified by column chromatography on silica gel (30–50% EtOAc in hexanes) to afford **41** (32 mg, 0.081 mmol, 39% yield) as a tan solid. ^1H NMR (400 MHz, $\text{DMSO}-d_6$) δ 11.83 (s, 1H), 9.37 (s, 1H), 9.03 (s, 1H), 8.78 (d, $J = 4.8$ Hz, 1H), 8.54 (d, $J = 5.0$ Hz, 1H), 7.91 (d, $J = 4.8$ Hz, 1H), 7.77–7.66 (m, 2H), 7.52–7.43 (m, 5H), 7.38 (dd, $J = 5.0, 1.8$ Hz, 3H), 7.35–7.27 (m, 1H). HRMS (ESI) m/z : 392.1499 [($\text{M} + \text{H}$) $^+$, calcd for $\text{C}_{24}\text{H}_{18}\text{N}_5\text{O}$ 392.1506]. HPLC purity: >98%, $t_{\text{R}} = 8.87$ min (method A); >98%, $t_{\text{R}} = 9.30$ min (method B).

N-(4-(4-Fluorophenyl)pyridin-3-yl)-2-phenylimidazo[1,2-b]pyridazine-8-carboxamide, 2 TFA (42). Compound **42** was prepared according to the procedure described for the synthesis of **36** using 2-phenylimidazo[1,2-b]pyridazine-8-carboxylic acid (**33a**) (30 mg, 0.125 mmol) and 4-(4-fluorophenyl)pyridin-3-amine (47.2 mg, 0.251 mmol). The product was purified by preparative reversed-phase HPLC (method A) and lyophilized to afford **42** (22 mg, 0.034 mmol, 27% yield) as a yellow solid. ^1H NMR (400 MHz, $\text{DMSO}-d_6$) δ 11.92 (s, 1H), 9.48 (s, 1H), 9.06 (s, 1H), 8.79 (d, $J = 4.8$ Hz, 1H), 8.59 (d, $J = 5.3$ Hz, 1H), 7.93 (d, $J = 4.8$ Hz, 1H), 7.86–7.80 (m, 2H), 7.62 (d, $J = 5.0$ Hz, 1H), 7.49–7.42 (m, 2H), 7.42–7.37 (m, 3H), 7.33–7.24 (m, 2H). HRMS (ESI) m/z : 410.1409 [($\text{M} + \text{H}$) $^+$, calcd for $\text{C}_{24}\text{H}_{17}\text{FN}_5\text{O}$ 410.1412]. HPLC purity: 100%, $t_{\text{R}} = 10.75$ min (method A); 100%, $t_{\text{R}} = 11.06$ min (method B).

2-Phenyl-N-(4-(piperidin-1-yl)pyridin-3-yl)imidazo[1,2-b]pyridazine-8-carboxamide, 2 TFA (43). Compound **43** was prepared according to the procedure described for the synthesis of **36** using 2-phenylimidazo[1,2-b]pyridazine-8-carboxylic acid (**33a**) (40 mg, 0.167 mmol) and 4-(piperidin-1-yl)pyridin-3-amine, HCl (84 mg, 0.334 mmol). The product was purified by preparative reversed-phase HPLC (method A) and lyophilized to afford **43** (41 mg, 0.063 mmol, 38% yield) as a tan solid. ^1H NMR (400 MHz, $\text{DMSO}-d_6$) δ 11.79 (s, 1H), 9.21 (s, 1H), 9.04 (d, $J = 0.5$ Hz, 1H), 8.84 (d, $J = 4.5$ Hz, 1H), 8.44 (dd, $J = 6.8, 1.0$ Hz, 1H), 8.26–8.12 (m, 2H), 7.94 (d, $J = 4.8$ Hz, 1H), 7.61–7.33 (m, 4H), 3.53–3.38 (m, 4H), 1.61 (br s, 4H), 1.46 (d, $J = 4.5$ Hz, 2H). HRMS (ESI) m/z : 399.1927 [($\text{M} + \text{H}$) $^+$, calcd for $\text{C}_{23}\text{H}_{23}\text{N}_6\text{O}$ 399.1928]. HPLC purity: 100%, $t_{\text{R}} = 16.70$ min (method A); 97.6%, $t_{\text{R}} = 18.07$ min (method B).

N-(4-(4,4-Difluoropiperidin-1-yl)pyridin-3-yl)-2-phenylimidazo[1,2-b]pyridazine-8-carboxamide, 2 TFA (44). Compound **44** was prepared according to the procedure described for the synthesis of **36** using 2-phenylimidazo[1,2-b]pyridazine-8-carboxylic acid (**33a**) (100 mg, 0.283 mmol) and 4-(4,4-difluoropiperidin-1-yl)pyridin-3-amine (72.4 mg, 0.340 mmol). The product was purified by preparative reversed-phase HPLC (method A) and lyophilized to afford **44** (58 mg, 0.125 mmol, 44% yield) as a yellow amorphous solid. ^1H NMR (400 MHz, $\text{DMSO}-d_6$) δ 11.77 (s, 1H), 9.21 (s, 1H), 9.17 (s, 1H), 8.83 (d, $J = 4.8$ Hz, 1H), 8.35 (d, $J = 5.5$ Hz, 1H), 8.17 (d, $J = 7.0$ Hz, 2H), 7.97 (d, $J = 4.8$ Hz, 1H), 7.58–7.50 (m, 2H), 7.48–7.42 (m, 1H), 7.27 (d, $J = 5.5$ Hz, 1H), 3.22 (t, $J = 5.0$ Hz, 4H), 2.10–1.95 (m, 4H). HRMS (ESI) m/z : 435.1736 [($\text{M} + \text{H}$) $^+$, calcd for $\text{C}_{23}\text{H}_{21}\text{F}_2\text{N}_6\text{O}$ 435.1939]. HPLC purity: 93.8%, $t_{\text{R}} = 10.26$ min (method A); 94.0%, $t_{\text{R}} = 10.24$ min (method B).

N-(4-Morpholinopyridin-3-yl)-2-phenylimidazo[1,2-b]pyridazine-8-carboxamide (45). Compound **45** was prepared according to the procedure described for the synthesis of **36** using 2-phenylimidazo[1,2-b]pyridazine-8-carboxylic acid (**33a**) (60 mg, 0.251 mmol) and 4-morpholinopyridin-3-amine (62.9 mg, 0.351

mmol). The product was purified by column chromatography on silica gel (20% EtOAc with 10% MeOH/80% hexanes–100% EtOAc with 10% MeOH) to afford **45** (58.5 mg, 0.146 mmol, 58% yield) as a yellow solid. ^1H NMR (500 MHz, $\text{DMSO}-d_6$) δ 11.80 (s, 1H), 9.16 (d, $J = 7.2$ Hz, 2H), 8.80 (d, $J = 4.7$ Hz, 1H), 8.36 (d, $J = 5.5$ Hz, 1H), 8.28–8.21 (m, 2H), 7.93 (d, $J = 4.7$ Hz, 1H), 7.57–7.52 (m, 2H), 7.48–7.42 (m, 1H), 7.23 (d, $J = 5.7$ Hz, 1H), 3.65–3.57 (m, 4H), 3.18–3.08 (m, 4H). ^{13}C NMR (126 MHz, $\text{DMSO}-d_6$) δ 159.8, 151.2, 146.7, 145.0, 144.8, 144.5, 137.3, 132.4, 129.5, 129.4, 127.0, 126.7, 118.9, 114.8, 114.3, 66.0, 50.5. HRMS (ESI) m/z : 401.1710 [($\text{M} + \text{H}$) $^+$, calcd for $\text{C}_{22}\text{H}_{21}\text{N}_6\text{O}_2$ 401.1721]. HPLC purity: 100%, $t_{\text{R}} = 9.18$ min (method A); 100%, $t_{\text{R}} = 9.79$ min (method B).

(S)-N-(4-(3-Methylmorpholino)pyridin-3-yl)-2-phenylimidazo[1,2-b]pyridazine-8-carboxamide, 2 TFA [(S)-46]. Compound **(S)-46** was prepared according to the procedure described for the synthesis of **36** using 2-phenylimidazo[1,2-b]pyridazine-8-carboxylic acid (**33a**) (40 mg, 0.167 mmol) and **(S)-4-(3-methylmorpholino)pyridin-3-amine** (64.6 mg, 0.334 mmol). The product was purified by preparative reversed-phase HPLC (method A) and lyophilized to afford **(S)-46** (36 mg, 0.055 mmol, 33% yield) as a yellow solid. ^1H NMR (400 MHz, $\text{DMSO}-d_6$) δ 11.86 (s, 1H), 9.28 (s, 1H), 9.17 (s, 1H), 8.81 (d, $J = 4.8$ Hz, 1H), 8.38 (d, $J = 5.5$ Hz, 1H), 8.27–8.21 (m, 2H), 7.94 (d, $J = 4.5$ Hz, 1H), 7.57–7.50 (m, 2H), 7.50–7.42 (m, 1H), 7.30 (d, $J = 5.5$ Hz, 1H), 3.66 (dd, $J = 11.2, 3.1$ Hz, 1H), 3.61–3.51 (m, 2H), 3.50–3.43 (m, 1H), 3.27–3.19 (m, 2H), 2.68 (td, $J = 7.8, 3.8$ Hz, 1H), 0.98 (d, $J = 6.3$ Hz, 3H). HRMS (ESI) m/z : 415.1868 [($\text{M} + \text{H}$) $^+$, calcd for $\text{C}_{23}\text{H}_{23}\text{N}_6\text{O}_2$ 415.1877]. HPLC purity: 100%, $t_{\text{R}} = 14.27$ min (method A); 100%, $t_{\text{R}} = 14.37$ min (method B).

(R)-N-(4-(3-Methylmorpholino)pyridin-3-yl)-2-phenylimidazo[1,2-b]pyridazine-8-carboxamide, 2 TFA [(R)-46]. Compound **(R)-46** was prepared according to the procedure described for the synthesis of **36** using 2-phenylimidazo[1,2-b]pyridazine-8-carboxylic acid (**33a**) (40 mg, 0.167 mmol) and **(R)-4-(3-methylmorpholino)pyridin-3-amine** (64.6 mg, 0.334 mmol). The product was purified by preparative reversed-phase HPLC (method A) and lyophilized to afford **(R)-46** (33 mg, 0.051 mmol, 30% yield) as a yellow solid. ^1H NMR (400 MHz, $\text{DMSO}-d_6$) δ 11.86 (s, 1H), 9.28 (s, 1H), 9.17 (s, 1H), 8.81 (d, $J = 4.8$ Hz, 1H), 8.38 (d, $J = 5.3$ Hz, 1H), 8.27–8.21 (m, 2H), 7.94 (d, $J = 4.8$ Hz, 1H), 7.57–7.50 (m, 2H), 7.50–7.42 (m, 1H), 7.30 (d, $J = 5.3$ Hz, 1H), 3.66 (dd, $J = 11.2, 3.1$ Hz, 1H), 3.61–3.50 (m, 2H), 3.50–3.40 (m, 1H), 3.27–3.17 (m, 2H), 2.73–2.64 (m, 1H), 0.98 (d, $J = 6.3$ Hz, 3H). HRMS (ESI) m/z : 415.1876 [($\text{M} + \text{H}$) $^+$, calcd for $\text{C}_{23}\text{H}_{23}\text{N}_6\text{O}_2$ 415.1877]. HPLC purity: 100%, $t_{\text{R}} = 12.77$ min (method A); 100%, $t_{\text{R}} = 14.12$ min (method B).

N-(4-(2-Methylmorpholino)pyridin-3-yl)-2-phenylimidazo[1,2-b]pyridazine-8-carboxamide (47). Compound **47** was prepared according to the procedure described for the synthesis of **36** using 2-phenylimidazo[1,2-b]pyridazine-8-carboxylic acid (**33a**) (30 mg, 0.125 mmol) and 4-(2-methylmorpholino)pyridin-3-amine (48.5 mg, 0.251 mmol). The product was purified by column chromatography on silica gel (30–50% EtOAc in hexanes) to afford **47** (22 mg, 0.053 mmol, 42% yield) as a yellow solid. ^1H NMR (500 MHz, $\text{DMSO}-d_6$) δ 11.79 (s, 1H), 9.18 (s, 1H), 9.14 (s, 1H), 8.80 (d, $J = 4.7$ Hz, 1H), 8.33 (d, $J = 5.4$ Hz, 1H), 8.21 (d, $J = 7.2$ Hz, 2H), 7.93 (d, $J = 4.7$ Hz, 1H), 7.56–7.50 (m, 2H), 7.48–7.42 (m, 1H), 7.19 (d, $J = 5.4$ Hz, 1H), 3.75–3.66 (m, 1H), 3.64–3.52 (m, 2H), 3.36–3.28 (m, 2H, partially obscured by the H_2O peak), 2.71 (td, $J = 11.6, 3.5$ Hz, 1H), 2.55 (d, $J = 11.4$ Hz, 1H), 0.94 (d, $J = 6.2$ Hz, 3H). ^{13}C NMR (126 MHz, $\text{DMSO}-d_6$) δ 159.8, 150.5, 147.5, 145.1, 145.0, 144.8, 137.3, 132.4, 129.5, 129.3, 127.3, 127.1, 126.7, 118.9, 114.8, 114.5, 71.1, 65.9, 56.2, 50.1, 19.0. HRMS (ESI) m/z : 415.1875 [($\text{M} + \text{H}$) $^+$, calcd for $\text{C}_{23}\text{H}_{23}\text{N}_6\text{O}_2$ 415.1877]. HPLC purity: 100%, $t_{\text{R}} = 9.41$ min (method A); 100%, $t_{\text{R}} = 9.85$ min (method B).

(S)-N-(4-(2-Methylmorpholino)pyridin-3-yl)-2-phenylimidazo[1,2-b]pyridazine-8-carboxamide [(S)-47] and (R)-N-(4-(2-Methylmorpholino)pyridin-3-yl)-2-phenylimidazo[1,2-b]pyridazine-8-carboxamide [(R)-47]. Racemic **N-(4-(2-methylmorpholino)pyridin-3-yl)-2-phenylimidazo[1,2-b]pyridazine-8-carboxamide (47)** (31 mg) was separated into its enantiomers by SFC chromatography (column: Chiraldak AS-H, 30 mm × 250 mm, 5 μm ;

mobile phase: 15% EtOH with 0.1% Et₂NH/85% CO₂; flow rate: 70 mL/min; 120 bar; 35 °C; λ = 370 nm) to afford (*S*)-47 (11 mg) (t_R = 12.68 min, peak 1) and (*R*)-47 (11 mg) (t_R = 14.25 min, peak 2).

(*S*)-*N*-(4-(2-Methylmorpholino)pyridin-3-yl)-2-phenylimidazo-[1,2-*b*]pyridazine-8-carboxamide [(*S*)-47]. [α]_D²² +55.7, (c = 0.190, MeOH). ¹H NMR (400 MHz, DMSO-*d*₆) δ 11.83 (s, 1H), 9.19 (d, J = 3.3 Hz, 2H), 8.82 (d, J = 4.8 Hz, 1H), 8.35 (d, J = 5.5 Hz, 1H), 8.27–8.22 (m, 2H), 7.95 (d, J = 4.8 Hz, 1H), 7.54 (t, J = 7.4 Hz, 2H), 7.49–7.44 (m, 1H), 7.21 (d, J = 5.3 Hz, 1H), 3.77–3.52 (m, 3H), 2.92–2.89 (m, 2H), 2.76–2.73 (m, 2H), 0.95 (d, J = 6.3 Hz, 3H). HRMS (ESI) *m/z*: 415.1864 [(M + H)⁺, calcd for C₂₃H₂₃N₆O₂ 415.1877]. HPLC purity: 100%, t_R = 8.55 min (method A); 100%, t_R = 9.76 min (method B). Analytical SFC chromatography (column: Chiralpak AS-H, 4.6 mm × 250 mm, 5 μ m; mobile phase: 15% EtOH with 0.1% Et₂NH/85% CO₂; 120 bar; 35 °C; flow rate: 3 mL/min; λ = 370 nm), t_R = 8.47 min.

(*R*)-*N*-(4-(2-Methylmorpholino)pyridin-3-yl)-2-phenylimidazo-[1,2-*b*]pyridazine-8-carboxamide [(*R*)-47]. [α]_D²² -46.8, (c = 0.210, MeOH). ¹H NMR (400 MHz, DMSO-*d*₆) δ 11.83 (s, 1H), 9.19 (d, J = 3.3 Hz, 2H), 8.82 (d, J = 4.8 Hz, 1H), 8.35 (d, J = 5.5 Hz, 1H), 8.27–8.22 (m, 2H), 7.95 (d, J = 4.8 Hz, 1H), 7.54 (t, J = 7.4 Hz, 2H), 7.49–7.44 (m, 1H), 7.21 (d, J = 5.3 Hz, 1H), 3.77–3.52 (m, 3H), 2.92–2.89 (m, 2H), 2.76–2.73 (m, 2H), 0.95 (d, J = 6.3 Hz, 3H). HRMS (ESI) *m/z*: 415.1876 [(M + H)⁺, calcd for C₂₃H₂₃N₆O₂ 415.1877]. HPLC purity: 100%, t_R = 9.42 min (method A); 100%, t_R = 9.89 min (method B). Analytical SFC chromatography (column: Chiralpak AS-H, 4.6 mm × 250 mm, 5 μ m; mobile phase: 25% EtOH with 0.1% Et₂NH/85% CO₂; 120 bar; 35 °C; flow rate: 3 mL/min; λ = 370 nm), t_R = 10.10 min.

(*S*)-*N*-(4-(2-Methylmorpholino)pyridin-3-yl)-2-phenylimidazo-[1,2-*b*]pyridazine-8-carboxamide [(*S*)-47]. (Prepared from 33a and (*S*)-4-(2-methylmorpholino)pyridin-3-amine.) Compound (*S*)-47 was prepared according to the procedure described for the synthesis of 36 using 2-phenylimidazo[1,2-*b*]pyridazine-8-carboxylic acid (33a) (60 mg, 0.251 mmol) and (*S*)-4-(2-methylmorpholino)pyridin-3-amine (67.9 mg, 0.351 mmol). The product was purified by column chromatography on silica gel (20% EtOAc with 10% MeOH/80% hexanes–100% EtOAc with 10% MeOH) to afford (*S*)-47 (61.7 mg, 0.149 mmol, 59% yield) as a yellow solid. [α]_D²² +48.4, (c = 0.295, MeOH). ¹H NMR (500 MHz, DMSO-*d*₆) δ 11.79 (s, 1H), 9.18 (s, 1H), 9.14 (s, 1H), 8.80 (d, J = 4.7 Hz, 1H), 8.33 (d, J = 5.4 Hz, 1H), 8.21 (d, J = 7.2 Hz, 2H), 7.93 (d, J = 4.7 Hz, 1H), 7.56–7.50 (m, 2H), 7.48–7.42 (m, 1H), 7.19 (d, J = 5.4 Hz, 1H), 3.75–3.66 (m, 1H), 3.64–3.52 (m, 2H), 3.36–3.28 (m, 2H), 2.71 (td, J = 11.6, 3.5 Hz, 1H), 2.55 (d, J = 11.4 Hz, 1H), 0.94 (d, J = 6.2 Hz, 3H). HRMS (ESI) *m/z*: 415.1865 [(M + H)⁺, calcd for C₂₃H₂₃N₆O₂ 415.1877]. HPLC purity: 100%, t_R = 1.36 min (method E); 100%, t_R = 1.37 min (method F).

(*R*)-*N*-(4-(2-Methylmorpholino)pyridin-3-yl)-2-phenylimidazo-[1,2-*b*]pyridazine-8-carboxamide [(*R*)-47]. (Prepared from 33a and (*R*)-4-(2-methylmorpholino)pyridin-3-amine.) Compound (*R*)-47 was prepared according to the procedure described for the synthesis of 36 using 2-phenylimidazo[1,2-*b*]pyridazine-8-carboxylic acid (33a) (60 mg, 0.251 mmol) and (*R*)-4-(2-methylmorpholino)pyridin-3-amine (67.9 mg, 0.351 mmol). The product was purified by column chromatography on silica gel (20% EtOAc with 10% MeOH/80% hexanes–100% EtOAc with 10% MeOH) to afford (*R*)-47 (65 mg, 0.157 mmol, 63% yield) as a yellow solid. [α]_D²² -46.3, (c = 0.280, MeOH). ¹H NMR (500 MHz, DMSO-*d*₆) δ 11.79 (s, 1H), 9.18 (s, 1H), 9.14 (s, 1H), 8.80 (d, J = 4.7 Hz, 1H), 8.33 (d, J = 5.4 Hz, 1H), 8.21 (d, J = 7.2 Hz, 2H), 7.93 (d, J = 4.7 Hz, 1H), 7.56–7.50 (m, 2H), 7.48–7.42 (m, 1H), 7.19 (d, J = 5.4 Hz, 1H), 3.75–3.66 (m, 1H), 3.64–3.52 (m, 2H), 3.36–3.28 (m, 2H), 2.71 (td, J = 11.6, 3.5 Hz, 1H), 2.55 (d, J = 11.4 Hz, 1H), 0.94 (d, J = 6.2 Hz, 3H). HRMS (ESI) *m/z*: 415.1868 [(M + H)⁺, calcd for C₂₃H₂₃N₆O₂ 415.1877]. HPLC purity: 100%, t_R = 1.31 min (method E); 100%, t_R = 1.33 min (method F).

2-(2-Methoxyphenyl)-*N*-(4-(2-methylmorpholino)pyridin-3-yl)-imidazo[1,2-*b*]pyridazine-8-carboxamide (48). Compound 48 was prepared according to the procedure described for the synthesis of 36

using 2-(2-methoxyphenyl)imidazo[1,2-*b*]pyridazine-8-carboxylic acid (33b) (15 mg, 0.056 mmol) and 4-(2-methylmorpholino)pyridin-3-amine (21.5 mg, 0.111 mmol). The product was purified by column chromatography on silica gel (20–80% EtOAc in hexanes) to afford 48 (10 mg, 0.022 mmol, 40% yield) as a yellow solid. ¹H NMR (400 MHz, CDCl₃) δ 12.03 (s, 1H), 9.40–9.31 (m, 1H), 8.75 (s, 1H), 8.56 (d, J = 4.5 Hz, 1H), 8.51 (dd, J = 7.8, 1.8 Hz, 1H), 8.41 (d, J = 5.5 Hz, 1H), 7.99 (d, J = 4.8 Hz, 1H), 7.44–7.39 (m, 1H), 7.10–7.04 (m, 2H), 7.02 (d, J = 5.5 Hz, 1H), 4.07 (s, 3H), 3.82–3.76 (m, 1H), 3.76–3.70 (m, 2H), 3.34–3.27 (m, 2H), 2.87 (ddd, J = 12.2, 10.2, 4.6 Hz, 1H), 2.64 (dd, J = 11.8, 10.3 Hz, 1H), 1.04 (d, J = 6.3 Hz, 3H). HRMS (ESI) *m/z*: 445.1974 [(M + H)⁺, calcd for C₂₄H₂₅N₆O₃ 445.1983]. HPLC purity: 100%, t_R = 9.76 min (method A); 100%, t_R = 10.19 min (method B).

N-(4-(2-Methylmorpholino)pyridin-3-yl)-2-(4-(trifluoromethyl)phenyl)imidazo[1,2-*b*]pyridazine-8-carboxamide (49). To a suspension of 2-(4-(trifluoromethyl)phenyl)imidazo[1,2-*b*]pyridazine-8-carboxylic acid (33c) (50 mg, 0.098 mmol) in CH₂Cl₂ (4 mL) at 0 °C was added DMF (1.5 μ L, 0.02 mmol) and oxalyl chloride (0.026 mL, 0.293 mmol). The reaction mixture was stirred at 22 °C for 1 h. The solvent was evaporated and the residue was dried under vacuum. The residue was suspended in CH₂Cl₂ (4 mL) at 0 °C and TEA (0.054 mL, 0.391 mmol), DMAP (23.9 mg, 0.195 mmol), and 4-(2-methylmorpholino)pyridin-3-amine (37.7 mg, 0.195 mmol) were added to the mixture. The reaction mixture was stirred at 22 °C for 4 h. The mixture was transferred to a separatory funnel containing saturated aqueous NaHCO₃ (15 mL). The aqueous layer was extracted with CH₂Cl₂ (3 × 15 mL). The combined organic layers were washed with brine (15 mL), dried over MgSO₄, filtered, and concentrated under vacuum. The product was purified by preparative reversed-phase HPLC (method A) and lyophilized. The product was purified further by preparative thin-layer chromatography (5% MeOH in CH₂Cl₂) to afford 49 (15 mg, 0.030 mmol, 30% yield) as a yellow solid. ¹H NMR (400 MHz, DMSO-*d*₆) δ 11.73 (s, 1H), 9.36 (s, 1H), 9.04 (br s, 1H), 8.88 (d, J = 4.5 Hz, 1H), 8.50 (br s, 1H), 8.46–8.41 (m, J = 8.0 Hz, 2H), 7.97 (d, J = 4.5 Hz, 1H), 7.94–7.90 (m, J = 8.3 Hz, 2H), 7.59 (br s, 1H), 3.95 (t, J = 13.8 Hz, 2H), 3.74–3.62 (m, 2H), 3.56 (t, J = 10.8 Hz, 1H), 3.14 (t, J = 10.9 Hz, 1H), 2.92–2.85 (m, 1H), 0.94 (d, J = 6.3 Hz, 3H). HRMS (ESI) *m/z*: 483.1736 [(M + H)⁺, calcd for C₂₄H₂₂F₃N₆O₂ 483.1756]. HPLC purity: 97%, t_R = 10.63 min (method A); 94.4%, t_R = 10.63 min (method B).

N-(4-Morpholinopyridin-3-yl)-2-(4-(trifluoromethyl)phenyl)-imidazo[1,2-*b*]pyridazine-8-carboxamide (50). To a suspension of 2-(4-(trifluoromethyl)phenyl)imidazo[1,2-*b*]pyridazine-8-carboxylic acid (33c) (30 mg, 0.059 mmol) in CH₂Cl₂ (4 mL) at 0 °C was added DMF (0.91 μ L, 0.012 mmol) and oxalyl chloride (0.015 mL, 0.176 mmol). The mixture was stirred at 22 °C for 1 h. The mixture was concentrated under vacuum. The residue was suspended in CH₂Cl₂ (4 mL) at 0 °C, and TEA (0.033 mL, 0.234 mmol), DMAP (14.3 mg, 0.117 mmol), and 4-morpholinopyridin-3-amine (21.0 mg, 0.117 mmol) were added to the mixture. The reaction mixture was stirred at 22 °C for 4 h. The mixture was transferred to a separatory funnel containing saturated aqueous NaHCO₃ (15 mL). The aqueous layer was extracted with CH₂Cl₂ (3 × 15 mL). The combined organic layers were washed with brine (15 mL), dried over MgSO₄, filtered, and concentrated under vacuum. The product was purified by preparative reversed-phase HPLC (method A). The product was purified further by preparative thin-layer chromatography (5% MeOH in CH₂Cl₂) to afford 50 (7 mg, 0.014 mmol, 24% yield) as a yellow solid. ¹H NMR (400 MHz, CD₃OD) δ 9.26 (br s, 1H), 8.89 (s, 1H), 8.71 (d, J = 4.6 Hz, 1H), 8.38 (br s, 1H), 8.37 (d, J = 8.1 Hz, 2H), 8.00 (d, J = 4.8 Hz, 1H), 7.84 (d, J = 8.1 Hz, 2H), 7.26 (br d, J = 1.5 Hz, 1H), 3.74–3.61 (m, 4H), 3.22–3.08 (m, 4H). ¹⁹F NMR (377 MHz, CDCl₃) δ -62.66 (s, 1F). HRMS (ESI) *m/z*: 469.1522 [(M + H)⁺, calcd for C₂₃H₂₀F₃N₆O₂ 469.1594]. HPLC purity: >99%, t_R = 11.23 min (method A); 95.5%, t_R = 10.73 min (method B).

N-(5-Methoxypyridin-3-yl)-2-phenylimidazo[1,2-*b*]pyridazine-8-carboxamide (51). Compound 51 was prepared according to the procedure described for the synthesis of 36 using 2-phenylimidazo[1,2-*b*]pyridazine-8-carboxylic acid (33a) (30 mg, 0.125 mmol) and

5-methoxypyridin-3-amine (31.1 mg, 0.251 mmol). The product was purified by column chromatography on silica gel (5% CH₂Cl₂ in MeOH) to afford **51** (21 mg, 0.060 mmol, 48% yield) as a yellow solid. ¹H NMR (400 MHz, DMSO-*d*₆) δ 12.13 (br s, 1H), 9.15 (s, 1H), 8.79 (d, *J* = 4.8 Hz, 1H), 8.54 (s, 1H), 8.23–8.17 (m, 3H), 8.06 (br s, 1H), 7.86 (d, *J* = 4.5 Hz, 1H), 7.57 (br t, *J* = 7.5 Hz, 2H), 7.48–7.42 (m, 1H), 3.92 (s, 3H). MS (ESI) *m/z*: 346.1 (M + H)⁺. HPLC purity: 100%, *t*_R = 10.50 min (method A); 99.0%, *t*_R = 10.52 min (method B).

N-(6-Chloro-4-(4,4-difluoropiperidin-1-yl)pyridin-3-yl)-2-phenylimidazo[1,2-*b*]pyridazine-8-carboxamide, TFA (**52**). Compound **52** was prepared according to the procedure described for the synthesis of **36** using 2-phenylimidazo[1,2-*b*]pyridazine-8-carboxylic acid (**33a**) (10 mg, 0.042 mmol) and 6-chloro-4-(4,4-difluoropiperidin-1-yl)pyridin-3-amine (10.4 mg, 0.042 mmol). The product was purified by reversed-phase HPLC (method A) to afford **52** (10 mg, 0.018 mmol, 42% yield) as a yellow solid. ¹H NMR (400 MHz, DMSO-*d*₆) δ 11.76 (s, 1H), 9.17 (s, 1H), 9.01 (s, 1H), 8.83 (d, *J* = 4.5 Hz, 1H), 8.15 (d, *J* = 7.0 Hz, 2H), 7.96 (d, *J* = 4.8 Hz, 1H), 7.56–7.50 (m, 2H), 7.48–7.42 (m, 1H), 7.33 (s, 1H), 3.27 (br t, *J* = 5.1 Hz, 4H), 2.07–1.95 (m, 4H). MS (ESI) *m/z*: 469.2 (M + H)⁺. HPLC purity: >99%, *t*_R = 17.06 min (method A); >99%, *t*_R = 15.53 min (method B).

2-Cyclopropyl-N-(4-(2-methylmorpholino)pyridin-3-yl)imidazo[1,2-*b*]pyridazine-8-carboxamide, 2 TFA (**53**). Compound **53** was prepared according to the procedure described for the synthesis of **36** using 2-cyclopropylimidazo[1,2-*b*]pyridazine-8-carboxylic acid (**34**) (35 mg, 0.172 mmol) and 4-(2-methylmorpholino)pyridin-3-amine (46 mg, 0.241 mmol). The product was purified by preparative reversed-phase HPLC (method A) and lyophilized to afford **53** (62.6 mg, 0.099 mmol, 58% yield) as a yellow amorphous solid. ¹H NMR (500 MHz, DMSO-*d*₆) δ 11.68 (s, 1H), 9.09 (s, 1H), 8.74 (d, *J* = 4.7 Hz, 1H), 8.47 (dd, *J* = 6.8, 0.8 Hz, 1H), 8.38 (s, 1H), 7.84 (d, *J* = 4.7 Hz, 1H), 7.53 (d, *J* = 6.8 Hz, 1H), 3.89–3.79 (m, 4H), 3.78–3.72 (m, 1H), 3.21–3.13 (m, 1H), 2.87 (dd, *J* = 12.7, 10.1 Hz, 1H), 2.20 (tt, *J* = 8.4, 5.0 Hz, 1H), 1.12–1.06 (m, 2H), 1.04 (d, *J* = 6.1 Hz, 3H), 0.99–0.94 (m, 2H). ¹⁹F NMR (471 MHz, DMSO-*d*₆) δ -74.16 (s, 1F). ¹³C NMR (126 MHz, DMSO-*d*₆) δ 160.7, 158.6 (q, *J* = 33.4 Hz, 1C, TFA salt), 155.4, 150.4, 144.2, 139.3, 137.8, 136.0, 125.7, 125.2, 117.9, 117.0 (q, *J* = 296.6 Hz, 1C, TFA salt), 114.9, 114.0, 71.3, 65.8, 55.2, 49.3, 18.9, 10.2, 9.3, 9.2. HRMS (ESI) *m/z*: 379.1870 [(M + H)⁺, calcd for C₂₀H₂₃N₆O₂ 379.1877]. HPLC purity: 96.4%, *t*_R = 8.45 min (method A); 96.8%, *t*_R = 8.74 min (method B).

2-Cyclopropyl-N-(4-(4,4-difluoropiperidin-1-yl)pyridin-3-yl)imidazo[1,2-*b*]pyridazine-8-carboxamide, 2 TFA (**54**). Compound **54** was prepared according to the procedure described for the synthesis of **36** using 2-cyclopropylimidazo[1,2-*b*]pyridazine-8-carboxylic acid (**34**) (35 mg, 0.172 mmol) and 4-(4,4-difluoropiperidin-1-yl)pyridin-3-amine (51.4 mg, 0.241 mmol). The product was purified by preparative reversed-phase HPLC (method A) and lyophilized to afford **54** (55.7 mg, 0.088 mmol, 51% yield) as a yellow amorphous solid. ¹H NMR (400 MHz, DMSO-*d*₆) δ 11.78 (s, 1H), 9.22 (s, 1H), 8.76 (d, *J* = 4.8 Hz, 1H), 8.53 (dd, *J* = 6.8, 1.0 Hz, 1H), 8.40 (s, 1H), 7.89 (d, *J* = 4.5 Hz, 1H), 7.63 (d, *J* = 6.5 Hz, 1H), 3.60 (t, *J* = 5.4 Hz, 4H), 2.31–2.13 (m, 5H), 1.12–1.05 (m, 2H), 0.98–0.91 (m, 2H). HRMS (ESI) *m/z*: 399.1741 [(M + H)⁺, calcd for C₂₀H₂₁F₂N₆O₂ 399.1739]. HPLC purity: >99%, *t*_R = 9.36 min (method A); >99%, *t*_R = 9.99 min (method B).

2-Cyclopropyl-N-(4-(4-fluorophenyl)pyridin-3-yl)imidazo[1,2-*b*]pyridazine-8-carboxamide, 2 TFA (**55**). Compound **55** was prepared according to the procedure described for the synthesis of **36** using 2-cyclopropylimidazo[1,2-*b*]pyridazine-8-carboxylic acid (**34**) (35 mg, 0.172 mmol) and 4-(4-fluorophenyl)pyridin-3-amine (45.5 mg, 0.241 mmol). The product was purified by preparative reversed-phase HPLC (method A) and lyophilized to afford **55** (43.3 mg, 0.071 mmol, 41% yield) as a yellow amorphous solid. ¹H NMR (400 MHz, DMSO-*d*₆) δ 11.74 (s, 1H), 9.48 (s, 1H), 8.70 (d, *J* = 4.8 Hz, 1H), 8.59 (d, *J* = 5.3 Hz, 1H), 8.26 (s, 1H), 7.83 (d, *J* = 4.8 Hz, 1H), 7.73–7.67 (m, 2H), 7.60 (d, *J* = 5.3 Hz, 1H), 7.41–7.33 (m, 2H), 1.79 (tt, *J* = 8.3, 5.0 Hz, 1H), 0.92–0.84 (m, 2H), 0.54–0.46 (m, 2H). HRMS

(ESI) *m/z*: 374.1409 [(M + H)⁺, calcd for C₂₁H₁₇FN₅O₂ 374.1412]. HPLC purity: 99.7%, *t*_R = 10.03 min (method A); 99.6%, *t*_R = 10.50 min (method B).

N-(4-(2-Methylmorpholino)pyridin-3-yl)imidazo[1,2-*b*]pyridazine-8-carboxamide, 2 TFA (**56**). Compound **56** was prepared according to the procedure described for the synthesis of **36** using imidazo[1,2-*b*]pyridazine-8-carboxylic acid (**35**) (30 mg, 0.108 mmol) and 4-(2-methylmorpholino)pyridin-3-amine (41.8 mg, 0.216 mmol). The product was purified by preparative reversed-phase HPLC (method A) and lyophilized to afford **56** (15 mg, 0.025 mmol, 23% yield) as a red solid. ¹H NMR (400 MHz, CDCl₃) δ 12.20 (br s, 1H), 9.69 (s, 1H), 8.65 (d, *J* = 4.5 Hz, 1H), 8.55 (br d, *J* = 6.5 Hz, 1H), 8.19 (d, *J* = 1.0 Hz, 1H), 8.02 (d, *J* = 4.5 Hz, 1H), 7.89 (d, *J* = 1.0 Hz, 1H), 7.32 (d, *J* = 6.8 Hz, 1H), 4.16–3.99 (m, 3H), 3.62 (br d, *J* = 12.3 Hz, 2H), 3.18 (td, *J* = 11.9, 3.3 Hz, 1H), 2.94–2.81 (m, 1H), 1.22 (d, *J* = 6.3 Hz, 3H). HRMS (ESI) *m/z*: 339.1565 [(M + H)⁺, calcd for C₁₇H₁₉N₆O₂ 339.1564]. HPLC purity: 95.0%, *t*_R = 6.71 min (method A); 98.4%, *t*_R = 7.21 min (method B).

N-(4-(4,4-Difluoropiperidin-1-yl)pyridin-3-yl)imidazo[1,2-*b*]pyridazine-8-carboxamide, 2 TFA (**57**). Compound **57** was prepared according to the procedure described for the synthesis of **36** using imidazo[1,2-*b*]pyridazine-8-carboxylic acid (**35**) (30 mg, 0.108 mmol) and 4-(4,4-difluoropiperidin-1-yl)pyridin-3-amine (46.2 mg, 0.216 mmol). The product was purified by preparative reversed-phase HPLC (method A) and lyophilized to afford **57** (17 mg, 0.029 mmol, 27% yield) as a yellow solid. ¹H NMR (400 MHz, DMSO-*d*₆) δ 12.02 (s, 1H), 9.32 (s, 1H), 8.87 (d, *J* = 4.8 Hz, 1H), 8.62 (d, *J* = 1.3 Hz, 1H), 8.53 (dd, *J* = 6.5, 0.8 Hz, 1H), 8.03 (d, *J* = 1.3 Hz, 1H), 7.97 (d, *J* = 4.5 Hz, 1H), 7.62 (d, *J* = 6.5 Hz, 1H), 3.56–3.50 (m, 4H), 2.32–2.19 (m, 4H). HRMS (ESI) *m/z*: 359.1418 [(M + H)⁺, calcd for C₁₇H₁₇F₂N₆O₂ 359.1426]. HPLC purity: >99%, *t*_R = 7.90 min (method A); >99%, *t*_R = 8.48 min (method B).

GSK-3 α/β Enzyme Assay. The kinase assay was performed in V-bottom 384-well plates. The final assay volume was 30 μ L prepared from 15 μ L additions of enzyme, substrates (fluoresceinated peptide FL-KRREILSRP[ps]ERYR-NH₂ and ATP), and test compounds in assay buffer (100 mM HEPES pH 7.4, 10 mM MgCl₂, 25 mM β -glycerolphosphate, 0.015% Brij35, and 0.25 mM DTT). The reaction was incubated at 22 °C for 20 h and terminated by adding 45 μ L of 35 mM EDTA to each sample. The reaction mixture was analyzed on the Caliper LabChip3000 (Caliper, Hopkinton, MA) by electrophoretic separation of the unphosphorylated substrate and phosphorylated product. Inhibition data were calculated by comparison of the no enzyme control reactions for 100% inhibition and vehicle-only reactions for 0% inhibition. The final concentration of reagents in the assay was 250 pM GSK-3 α (Invitrogen: PV6126, Recombinant human full-length protein, GST-tagged) or GSK-3 β (Upstate: 14-306, N-terminal 6Histagged recombinant GST-3B with an H355L mutation), 20 μ M ATP, 1.5 μ M FL-KRREILSRP[ps]ERYR-NH₂, and 1.6% DMSO. Dose-response curves were generated to determine the concentration required to inhibit 50% of the kinase activity (IC₅₀). Compounds were dissolved at 10 mM in dimethyl sulfoxide (DMSO) and evaluated at eleven concentrations IC₅₀ values were derived by nonlinear regression analysis.

pTau Cellular Assay. The ability of GSK-3 inhibitors to modulate Tau phosphorylation at a preferred GSK-3 site (S396) was measured in a high-content imaging assay. U2OS/ β -catenin-GFP cells (Bio-Image) transfected with 4R1N tau plasmid were seeded into 384-well plates (Falcon 353962) at a concentration of 3000 cells/well. Compounds serial diluted in DMSO were added to a final concentration of 0.33% DMSO, and plates were incubated overnight. Cells were fixed with 8% formaldehyde in phosphate-buffered saline (PBS) (Cellgro 21-030-CM) containing 20 μ g/mL Hoechst, washed twice with PBS, permeabilized with 0.1% Triton X-100 in PBS, washed three times with PBS and nonspecifically blocked with 0.1% bovine serum albumin in PBS for 1 h with gentle shaking. Anti-[pS396]Tau (Biosource 44-752G) and anti-Tau (Biosource AHB0042) primary antibodies were added and plates were incubated for 1 h with gentle shaking. Wells were washed three times with PBS, secondary antibodies (Molecular Probes A21236 and 33342) were

added, and incubated for 1 h with gentle shaking. Plates were washed three times with PBS, sealed, and read on a Cellomics Array Scan using a Compartmental Analysis Bioapplication. Cells not expressing total Tau were gated out before analysis of Tau phosphorylated at S396. Dose-response curves were fit using a nonlinear regression model and the IC_{50} value was determined at the value of X at $Y = 50\%$. Each IC_{50} run represents the analysis of triplicate plates for each compound.

X-ray Crystallography. The GSK-3 β protein was expressed and purified as previously described.⁴⁹ GSK-3 β was mixed with a 10-fold molar excess of compound 22 (1 mM final concentration in DMSO). Crystals were grown at 20 °C by vapor diffusion in the presence of 20% w/v PEG 6000, 0.2 M ammonium chloride, and 0.1 M MES pH 6.0. Crystals would nucleate within 1–3 days and continued to grow for an additional 5–10 days before harvesting. Crystals were cryoprotected in a solution consisting of the mother liquor, glycerol, and PEG 400. Crystals were coated lightly with medium-weight immersion oil and flash-frozen in liquid nitrogen. The coordinates of the complex GSK-3 β :compound 22 have been deposited in the PDB under PDB ID 8DJE.

GSK-3 β was mixed with a 10-fold molar excess of compound 47 (1 mM final concentration in DMSO). Crystals were grown at 20 °C by vapor diffusion in the presence of 20% w/v PEG 3350 and 0.1 M lithium chloride. Crystals would nucleate within 1–3 days and continued to grow for an additional 5–10 days before harvesting. Crystals were cryoprotected in a solution consisting of the mother liquor, glycerol, and PEG 400. Crystals were coated lightly with medium-weight immersion oil and flash-frozen in liquid nitrogen. The coordinates of the complex GSK-3 β :compound 47 have been deposited in the PDB under PDB ID 8DJC.

Metabolic Stability in Liver Microsomes.⁶⁹ The metabolic stability (Metstab) assay evaluates cytochrome P450 (CYP)-mediated metabolism of test compounds in vitro using human and mouse microsomes after a 10 min incubation. The incubation was automated on a Biomek FX automation workstation (Beckman Coulter, Fullerton, CA). Each compound was incubated in duplicate in the respective species at a concentration of 0.5 μ M. Compounds were received as 3.5 mM solutions in DMSO and were diluted with CH₃CN to 50 μ M before being added to the prewarmed (37 °C) microsomal suspension (1 mg/mL) prepared in 100 mM sodium phosphate, pH 7.4, and 6.6 mM MgCl₂. The reaction was initiated by adding 17 μ L of prewarmed 5 mM NADPH in 100 mM sodium phosphate, pH 7.4, into 153 μ L of reaction mix. The concentration of DMSO in the incubation mixture was 0.014%. Reaction components were mixed well, and 75 μ L was transferred into 150 μ L of quench solution at 0 min time point (t_0) and again at the 10 min incubation time point (t_{10}). Quenched mixtures were centrifuged at 1500 rpm in an Allegra X-12 centrifuge (Beckman Coulter) for 15 min, and 90 μ L of the supernatant was then transferred to a separate 96-well plate for analysis. Metabolism rate was determined based on the parent compound disappearance over time, as measured by liquid chromatography–tandem mass spectrometry (LC–MS/MS).

Serum Protein Binding Assay. The serum protein binding assay was performed using a standard equilibrium dialysis method. In brief, stock solution of compounds was prepared by solubilizing in 100% DMSO (1 mM). These were spiked in serum so that the final test compound concentration was 10 μ M (final DMSO concentration 1%). Serum with compound was added to one of two chambered rapid equilibrium dialysis (RED) assay plates (8000-dalton molecular weight cut-off) and sodium phosphate buffer was added to the other chamber. Dialysis was performed at 37 °C for 5 h in a 10% CO₂ atmosphere. Samples were collected from serum and buffer chambers at pre- and post-incubation periods. These were analyzed using liquid chromatography with tandem mass spectrometry (LC–MS/MS) to evaluate the fraction of compound (percentage) free to diffuse and equilibrate between the buffer and serum chambers in the RED device. Percent free was calculated using the ratio of compound concentration in buffer to compound concentration in serum at the end of the dialysis period (5 h).

Brain Tissue Binding Assay. Mouse brain homogenates were harvested and prepared from frozen brain tissue and diluted 20 \times with Dulbecco's phosphate-buffered saline (DPBS). A Rapid Equilibrium Dialysis (RED) device (Thermo Fisher Scientific, Waltham, MA) was used according to vendor instructions as follows. Brain homogenate was spiked with compounds at a final concentration of 1 μ M. A 200- μ L aliquot of brain homogenate spiked with 1 μ M of compound was added to one side of the chamber (donor), and 350 μ L of DPBS was added to the other side of the dialysis insert (receiver). Compounds were assessed in triplicate (using 3 RED inserts for each experiment) to determine the extent of brain tissue binding. The RED plate was covered with a sealing tape obtained from Thermo Fisher Scientific and placed on a shaking plate at 350 rpm and incubated at 37 °C for 4 h. After incubation, 50 μ L was removed from both the donor and receiver wells and each sample matched with 50 μ L of opposite matrix before quenching with MeCN containing internal standard. Samples were then filtered and analyzed by LC/MS.

PAMPA Assay. Compounds and controls are utilized as 10 mM stocks in 100% DMSO. Compounds are diluted 1:100 in pH 7.4 or 5.5 donor-well buffer (pION, catalogue no. 110151), providing a 100 μ M assay solution in 1% DMSO. Compounds diluted in donor-well buffer were transferred to Whatman Unifilter plates and filtered prior to 200 μ L being dispensed into the donor wells of the assay plates (pION, catalogue no. 110163). The PAMPA membrane was formed by pipetting 4 μ L of the lipid solution (pION, catalogue no. 110169) onto the filter plate (VWR CAT #13503). The membrane was then covered with 200 μ L of acceptor-well buffer at pH 7.4 (pION, catalogue no. 110139). The PAMPA assay plate (donor and acceptor sides) was combined and allowed to incubate at 22 °C for 4 h. The plate was then disassembled and spectrophotometer plates (VWR, catalogue no. 655801) were filled (150 μ L/well). The donor, acceptor, reference, and blank plates were read in a SpectraMax UV plate reader. Data were captured by the pION software, which analyzed the spectra and generated P_c values.

Caco-2 Assay.^{70,71} Caco-2 cells were seeded on collagen-coated polycarbonate 24-well transwell plates and cultured to grow for 21 days to form a confluent monolayer. The monolayer integrity was assessed using a transepithelial electric resistance (TEER) before commencing the assay to ensure that it met acceptable criteria (>600 $\Omega\text{-cm}^2$). A stock solution of test compounds was prepared in dimethyl sulfoxide (DMSO) and these were spiked in assay buffer Hanks balanced salt solution (HBSS) containing 0.5% bovine serum albumin (pH 7.4). The final concentration of test compounds in assay buffer was 3 μ M. The bidirectional permeability assay [apical to basolateral (A–B) and basolateral to apical (B–A)] was conducted by adding the compound in assay buffer on the donor side and blank buffer on the receiver side. The volume added to the apical side was 200 μ L and to the basolateral side was 600 μ L. Transwell plates were incubated for 2 h at 37 °C in a 95% humidity and 5% CO₂ atmosphere. Aliquots (100 μ L) were collected from each apical and basolateral compartment. These aliquots were quenched with MeCN/MeOH (1:1) containing internal standard and were analyzed by LC–MS/MS to assess permeability. The control compounds used in this assay along with the typical range for each compound are as follows: digoxin, nadolol, verapamil, atenolol (pH 7.4, P_c A–B/B–A (10^{-6} cm/s)); 0–2.5/10.0–30.0 (low permeability, P-gp effluxed), 0–4.0/0–4.0 (low permeability), 10.0–40.0/10.0–40.0 (high permeability), 0–4.0/0–4.0 (low permeability), respectively.

Thermodynamic Equilibrium Aqueous Solubility Assay. HPLC-grade solvents were used for this assay.

Standards Preparation. A calibration standard was prepared by accurately weighing 0.3–0.7 mg of sample into a 5 mL volumetric flask which was then dissolved in pure methanol. If the standard material is not fully soluble in methanol, other solvents such as DMSO or a mixed solvent system can be used. The calibration standard must be fully dissolved, and a single-point calibration curve should be used to determine the concentration of the final solution. The calibration standard is typically prepared fresh before the start of the assay.

Test Sample Preparation. The final saturated solution was prepared by adding 1.0 mL of the appropriate aqueous solvent [pH 1 solution, pH 7.4 potassium phosphate buffer, fasted state simulated intestinal fluid (FaSSIF) (pH 6.5), or fed state simulated intestinal fluid (FeSSIF) (pH 5)] to ~1 mg of test compound (~1 mg/1 mL) in a 1 dram vial. The solution was sonicated and vortexed for ~30 s. The sample solution was placed on an orbiter that continually agitates the sample solutions for 18–24 h at room temperature. The final saturated solution was then transferred into a 1.5 mL Eppendorf tube and centrifuged at 10,000 rpm for ~2 min. The supernatant from the saturated solution was filtered, using a 0.45 μm poly(tetrafluoroethylene) (PTFE) syringe filter, into a 1.5 mL glass HPLC vial.

LC Quantitation. The standards and sample were analyzed by HPLC using either UV/visible diode array or variable wavelength detection. Typical quantitation wavelengths are 210 or 254 nm. Detection wavelength can be individually customized to optimize sensitivity. In addition to UV detection, mass spectrometry detection is recommended if available to confirm the identity of the HPLC-UV peak of interest. Dilutions of saturated aqueous test solutions were performed if the HPLC-UV peak was beyond the linear portion of the standard calibration curve. Typical dilutions include 100 μL /900 μL (10 \times) or 500 μL /500 μL (2 \times), as required.

Mouse Pharmacokinetic Studies. All animal experiments were performed in accordance with protocols approved by the Institutional Animal Ethics Committee and in a facility accredited by the Association for Assessment and Accreditation of Laboratory Animal Care (AAALAC) and registered by the Committee for the Purpose of Control and Supervision on Experiments on Animals (CPCSEA). Studies were conducted at Syngene International Ltd., Biocon-Bristol Myers Squibb Research Center, Bangalore, India. The pharmacokinetic studies were conducted in male C57BL6 mice (25 to 30 g, 12–14 weeks of age) purchased from Taconic Ltd. The animals were housed at $22 \pm 3^\circ\text{C}$ at a relative humidity of $50 \pm 20\%$ on a 12 h light and dark cycle and fed a standard laboratory rodent diet (Tetragon Chemie Pvt. Ltd, Bangalore). For oral pharmacokinetic studies, the mice were kept for 8 h fasting prior to formulation administration. Water was provided ad libitum throughout the study. Compounds formulated as solution were dosed as bolus via intravenous and oral routes of administration to mice at a dose of 2 and 10 mg/kg, respectively. Each sample was dosed in triplicate for intravenous and oral routes of administration. Blood samples were collected from retroorbital plexus by sparse sampling design. Tubes containing blood samples were centrifuged at 10,000g for 5 min at 4°C to collect plasma and stored at -80°C until analysis.

Bioanalytical Method Details. Sample Preparation. The study samples and calibration curves were prepared using the protein precipitation method. Calibration curves were prepared using serial dilution method in blank C57BL6 male mouse plasma in the concentration range of 0.61–5000 nM. MeCN (150 μL) containing internal standard (Ritonavir, 400 nM) was used to precipitate plasma sample (35 μL) in 96-well hydrophilic solvint plates (Millipore Corporation, Cat No: MSRL N04 50, Tullagreen, Carrigtwohill, Co Cork Ireland). The samples were vortex mixed at 300 rpm for 10 min and then centrifuged at 4000 rpm for 5 min at 4°C . Filtrates were collected in a 96-well, 1 mL round collection plate and analyzed by UPLC–MS/MS.⁷²

Inhibition of Tau Phosphorylation Studies. All animals were kept in an American Association for the Accreditation of Laboratory Animal Care-accredited animal holding facility maintained at controlled temperature ($23 \pm 1^\circ\text{C}$) and humidity ($50 \pm 20\%$). The mice were housed with a 6 AM–6 PM light/dark cycle and allowed free access to food and water. All experimental procedures were reviewed and approved by the Institutional Animal Ethics Committee and conducted in accordance with procedures set by the Committee for the Purpose of Control and Supervision on Experiments on Animals. 3xTg mice were obtained from Dr. Frank LaFerla at the University of California, Irvine. The mice were bred onto the C57BL6 background by Dr. Mark Mattson (National Institute on Aging) and breeders from those congenic mice were

obtained by BMS, where they were bred as homozygotes. Male animals between the ages of five to seven months were used for the study. Test compounds were dosed orally at 30 mg/kg as a solution in 83.4% PEG400/14.7% 50 mM Citrate (pH 3.0)/2% PVP-K30. LiCl was administered at 250 mg/kg by intraperitoneal injection in water. Animals were euthanized by guillotine 5 h post dose. Brains were dissected into hemispheres, flash-frozen in liquid nitrogen, and stored at -80°C until processing. Each hemisphere was homogenized in T-PER tissue protein extraction buffer (Thermo Scientific, Rockford, IL) supplemented with phosphatase inhibitor cocktail sets I and II (Sigma-Aldrich, St. Louis, MO), complete protease inhibitor EDTA-free (Roche, Indianapolis, IN) 7 μM pepstatin (Sigma-Aldrich, St. Louis, MO) and 1 mM PMSF (Sigma, St. Louis, MO) using a Potter-Elvehjem homogenizer. Homogenate was centrifuged at 100,000g for 30 min at 4°C . Cleared homogenate was frozen and stored at -80°C . Commercial total Tau human (KHB0041) and Tau[S396] human (KHB7031) ELISA kits (Invitrogen, Grand Island, NY) were used as directed to determine total and S396 phosphorylated human Tau levels in the cleared homogenates, respectively. Each sample was tested in triplicate, and compound-treated animal groups were compared to vehicle-treated animal groups with statistical analysis using Student's *t* test.

ASSOCIATED CONTENT

Supporting Information

The Supporting Information is available free of charge at <https://pubs.acs.org/doi/10.1021/acs.jmedchem.3c00133>.

Experimental procedures for the synthesis of 3-amino-pyridine intermediates; crystallographic data and refinement statistics for the X-ray crystal structures of **9**, **22**, and **47** complexed with GSK-3 β ; the kinase panel heat maps for **44**, **45**, and **47**; mouse pharmacokinetic profile of compound **47**; experimental UPLC–MS/MS analysis details for the mouse pharmacokinetic studies; and analytical HPLC traces and NMR spectra for compounds **45**, **47**, and **53** (PDF)

Molecular formula strings and SAR data (CSV)

Accession Codes

Atomic coordinates for the X-ray crystal structures of compounds **9** (PDB ID: 8DJD), **22** (PDB ID: 8DJE), and **47** (PDB ID: 8DJC) complexed with GSK-3 β are available from the RSCB Protein Data Bank (www.rcsb.org). The authors will release the atomic coordinates and experimental data upon article publication.

AUTHOR INFORMATION

Corresponding Author

Richard A. Hartz – Department of Small Molecule Drug Discovery, Bristol Myers Squibb, Research and Development, Wallingford, Connecticut 06492, United States; Present Address: Department of Small Molecule Drug Discovery, Bristol Myers Squibb, Research and Development, P.O. Box 5400, Princeton, New Jersey 08543, United States; orcid.org/0000-0002-3880-6646; Phone: 609-252-6107; Email: richard.hartz@bms.com

Authors

Vijay T. Ahuja – Department of Small Molecule Drug Discovery, Bristol Myers Squibb, Research and Development, Wallingford, Connecticut 06492, United States
Prasanna Sivaprakasam – Department of Molecular Structure and Design, Bristol Myers Squibb, Research and Development, Wallingford, Connecticut 06492, United States; orcid.org/0000-0002-4115-5055

Hong Xiao — Department of Neuroscience Discovery Biology, Bristol Myers Squibb, Research and Development, Wallingford, Connecticut 06492, United States

Carol M. Krause — Department of Neuroscience Discovery Biology, Bristol Myers Squibb, Research and Development, Wallingford, Connecticut 06492, United States

Wendy J. Clarke — Department of Metabolism and Pharmacokinetics, Bristol Myers Squibb, Research and Development, Wallingford, Connecticut 06492, United States

Kevin Kish — Department of Molecular Structure and Design, Bristol Myers Squibb, Research and Development, Princeton, New Jersey 08543, United States

Hal Lewis — Department of Molecular Structure and Design, Bristol Myers Squibb, Research and Development, Princeton, New Jersey 08543, United States

Nicolas Szapiel — Department of Protein Science, Bristol Myers Squibb, Research and Development, Princeton, New Jersey 08543, United States

Ramu Ravirala — Biocon-Bristol Myers Squibb Research and Development Center, Bangalore 560099, India

Sayali Mutualik — Biocon-Bristol Myers Squibb Research and Development Center, Bangalore 560099, India

Deepa Nakmode — Biocon-Bristol Myers Squibb Research and Development Center, Bangalore 560099, India

Devang Shah — Biocon-Bristol Myers Squibb Research and Development Center, Bangalore 560099, India

Catherine R. Burton — Department of Neuroscience Discovery Biology, Bristol Myers Squibb, Research and Development, Wallingford, Connecticut 06492, United States

John E. Macor — Department of Small Molecule Drug Discovery, Bristol Myers Squibb, Research and Development, Wallingford, Connecticut 06492, United States

Gene M. Dubowchik — Department of Small Molecule Drug Discovery, Bristol Myers Squibb, Research and Development, Wallingford, Connecticut 06492, United States

Complete contact information is available at:
<https://pubs.acs.org/10.1021/acs.jmedchem.3c00133>

Notes

The authors declare no competing financial interest.
All animal experiments performed were conducted in compliance with institutional guidelines.

ACKNOWLEDGMENTS

The authors thank Javed Khan and Matthew Pokross for assistance with refinement of the X-ray co-crystal structures, Anthony Paiva and Benjamin Johnson for conducting the metabolic ID study, and Tara Simmons for measuring the brain tissue homogenate unbound fraction.

ABBREVIATIONS USED

AAK1, adaptor protein 2-associated kinase 1 or adaptor-associated kinase 1; ATM, atmosphere; AUC_{tot}, area under the curve; B/P, brain-to-plasma; CDK2, cyclin-dependent kinase-2; CLK, CDC-like kinase; CMGC, a kinase family named after the initials of its subfamily members, including cyclin-dependent kinase (CDK), mitogen-activated protein kinase (MAPK), glycogen synthase kinase (GSK), and CDC-like kinase (CLK); CNS, central nervous system; DIPEA, N,N-diisopropylethylamine; DMAP, 4-dimethylaminopyridine; DMF, dimethylformide; DMSO, dimethyl sulfoxide; EDC, 1-ethyl-3-(3-dimethylaminopropyl)carbodiimide; EtOH, etha-

nol; EtOAc, ethyl acetate; Et₂O, diethyl ether; FaSSIF, fasted state simulated intestinal fluid; FeSSIF, fed state simulated intestinal fluid; GSH, glutathione; GSK-3, glycogen synthase kinase-3; HATU, hexafluorophosphate azabenzotriazole tetramethyl uronium; HPLC, high-performance liquid chromatography; IP, intraperitoneal; IV, intravenous; MAPK, mitogen-activated protein kinase; MeCN, acetonitrile; MeOH, methanol; MRT, mean residence time; NFTs, neurofibrillary tangles; PEG, poly(ethylene glycol); Pgp, P-glycoprotein; PKC θ , protein kinase C theta; PO, oral; PSI, pounds per square inch; pTau, phosphorylated tau; PVP, poly(vinyl pyrrolidone); SAR, structure–activity relationships; SFC, supercritical fluid chromatography; TEA, triethylamine; TFA, trifluoroacetic acid; THF, tetrahydrofuran; TLC, thin-layer chromatography

REFERENCES

- (1) Hardy, J. A hundred years of Alzheimer's disease research. *Neuron* **2006**, *52*, 3–13.
- (2) Alzheimer's Association. 2020 Alzheimer's disease facts and figures. *Alzheimer's Dement.* **2020**, *16*, 391–460.
- (3) Wadhwa, P.; Jain, P.; Jadhav, H. R. Glycogen synthase kinase 3 (GSK3): its role and inhibitors. *Curr. Top. Med. Chem.* **2020**, *20*, 1522–1534.
- (4) Jack, C. R.; Lowe, V. J.; Weigand, S. D.; Wiste, H. J.; Senjem, M. L.; Knopman, D. S.; Shiung, M. M.; Gunter, J. L.; Boeve, B. F.; Kemp, B. J.; Weiner, M.; Petersen, R. C. Serial PIB and MRI in normal, mild cognitive impairment and Alzheimer's disease: implications for sequence of pathological events in Alzheimer's disease. *Brain* **2009**, *132*, 1355–1365.
- (5) Yankner, B. A. Mechanisms of neuronal degeneration in Alzheimer's disease. *Neuron* **1996**, *16*, 921–932.
- (6) Embi, N.; Rylatt, D. B.; Cohen, P. Glycogen synthase kinase-3 from rabbit skeletal muscle. Separation from cyclic-AMP-dependent protein kinase and phosphorylase kinase. *Eur. J. Biochem.* **1980**, *107*, 519–527.
- (7) Sutherland, C. What are the *bona fide* GSK3 substrates? *Int. J. Alzheimer's Dis.* **2011**, *2011*, No. 505607.
- (8) Grimes, C. A.; Jope, R. S. The multifaceted roles of glycogen synthase kinase 3 β in cellular signaling. *Prog. Neurobiol.* **2001**, *65*, 391–426.
- (9) Tejeda-Muñoz, N.; Robles-Flores, M. Glycogen synthase kinase 3 in Wnt signaling pathway and cancer. *IUBMB Life* **2015**, *67*, 914–922.
- (10) Avila, J.; Wandosell, F.; Hernández, F. Role of glycogen synthase kinase-3 in Alzheimer's disease pathogenesis and glycogen synthase kinase-3 inhibitors. *Expert Rev. Neurother.* **2010**, *10*, 703–710.
- (11) Hanger, D. P.; Noble, W. Functional implications of glycogen synthase kinase-3-mediated tau phosphorylation. *Int. J. Alzheimer's Dis.* **2011**, *2011*, No. 352805.
- (12) Cai, Z.; Zhao, Y.; Zhao, B. Roles of glycogen synthase kinase 3 in Alzheimer's disease. *Curr. Alzheimer Res.* **2012**, *9*, 864–879.
- (13) Llorens-Martín, M.; Jurado, J.; Hernández, F.; Avila, J. GSK3 β , a pivotal kinase in Alzheimer disease. *Front. Mol. Neurosci.* **2014**, *7*, 00046.
- (14) Maqbool, M.; Mobashir, M.; Hoda, N. Pivotal role of glycogen synthase kinase-3: A therapeutic target for Alzheimer's disease. *Eur. J. Med. Chem.* **2016**, *107*, 63–81.
- (15) Maqbool, M.; Hoda, N. GSK3 inhibitors in the therapeutic development of diabetes, cancer and neurodegeneration: past, present and future. *Curr. Pharm. Des.* **2017**, *23*, 4332–4350.
- (16) Nikouline, S. E.; Ciaraldi, T. P.; Mudaliar, S.; Mohideen, P.; Carter, L.; Henry, R. R. Potential role of glycogen synthase kinase-3 in skeletal muscle insulin resistance of type 2 diabetes. *Diabetes* **2000**, *49*, 263–266.

- (17) Sahin, I.; Eturi, A.; De Souza, A.; Pamarthi, S.; Tavora, F.; Giles, F. J.; Carneiro, B. A. Glycogen synthase kinase-3 beta inhibitors as novel cancer treatments and modulators of antitumor immune responses. *Cancer Biol. Ther.* **2019**, *20*, 1047–1056.
- (18) Rowe, M. K.; Wiest, C.; Chuang, D. M. GSK-3 is a viable potential target for therapeutic intervention in bipolar disorder. *Neurosci. Biobehav. Rev.* **2007**, *31*, 920–931.
- (19) Lal, H.; Ahmad, F.; Woodgett, J.; Force, T. The GSK-3 family as therapeutic target for myocardial diseases. *Circ. Res.* **2015**, *116*, 138–149.
- (20) Woodgett, J. R. Molecular cloning and expression of glycogen synthase kinase-3/factor A. *EMBO J.* **1990**, *9*, 2431–2438.
- (21) Saeki, K.; Machida, M.; Kinoshita, Y.; Takasawa, R.; Tanuma, S. Glycogen synthase kinase-3 β 2 has lower phosphorylation activity to tau than glycogen synthase kinase-3 β 1. *Biol. Pharm. Bull.* **2011**, *34*, 146–149.
- (22) Pei, J. J.; Tanaka, T.; Tung, Y. C.; Braak, E.; Iqbal, K.; Grundke-Iqbali, I. Distribution, levels, and activity of glycogen synthase kinase-3 in the Alzheimer disease brain. *J. Neuropathol. Exp. Neurol.* **1997**, *56*, 70–78.
- (23) Pei, J. J.; Braak, E.; Braak, H.; Grundke-Iqbali, I.; Iqbal, K.; Winblad, B.; Cowburn, R. F. Distribution of active glycogen synthase kinase 3 β (GSK-3 β) in brains staged for Alzheimer disease neurofibrillary changes. *J. Neuropathol. Exp. Neurol.* **1999**, *58*, 1010–1019.
- (24) Leroy, K.; Brion, J.-P. Developmental expression and localization of glycogen synthase kinase-3 β in rat brain. *J. Chem. Neuroanat.* **1999**, *16*, 279–293.
- (25) Buée, L.; Bussière, T.; Buee-Scherrer, V.; Delacourte, A.; Hof, P. R. Tau protein isoforms, phosphorylation and role in neurodegenerative disorders. *Brain Res. Rev.* **2000**, *33*, 95–130.
- (26) Stebbings, H. Microtubule-based intracellular transport of organelles. In *Role in Cell Physiology*; Elsevier, 1995; Vol. 2, pp 113–140.
- (27) Burgess, S.; Geddes, J.; Hawton, K.; Townsend, E.; Jamison, K.; Goodwin, G. Lithium for maintenance treatment of mood disorders. *Cochrane Database Syst. Rev.* **2001**, No. CD003013.
- (28) Jope, R. S. Lithium and GSK-3: one inhibitor, two inhibitory actions, multiple outcomes. *Trends Pharmacol. Sci.* **2003**, *24*, 441–443.
- (29) Meijer, L.; Flajolet, M.; Greengard, P. Pharmacological inhibitors of glycogen synthase kinase 3. *Trends Pharmacol. Sci.* **2004**, *25*, 471–480.
- (30) Caccamo, A.; Oddo, S.; Tran, L. X.; LaFerla, F. M. Lithium reduces tau phosphorylation but not A β or working memory deficits in a transgenic model with both plaques and tangles. *Am. J. Pathol.* **2007**, *170*, 1669–1675.
- (31) Noble, W.; Planell, E.; Zehr, C.; Olm, V.; Meyerson, J.; Suleiman, F.; Gaynor, K.; Wang, L.; LaFrancois, J.; Feinstein, B.; Burns, M.; Krishnamurthy, P.; Wen, Y.; Bhat, R.; Lewis, J.; Dickson, D.; Duff, K. Inhibition of glycogen synthase kinase-3 by lithium correlates with reduced tauopathy and degeneration in vivo. *Proc. Natl. Acad. Sci. U.S.A.* **2005**, *102*, 6990–6995.
- (32) Liu, S.-K.; Xie, H.-X.; Ge, Y.-X.; Zhang, J.; Jiang, C.-S. An updated research of glycogen synthase kinase-3 β inhibitors: a review. *Monatsh. Chem.* **2021**, *152*, 19–33.
- (33) Roca, C.; Campillo, N. E. Glycogen synthase kinase 3 (GSK-3) inhibitors: a patent update (2016–2019). *Expert Opin. Ther. Pat.* **2020**, *30*, 863–872.
- (34) Xu, M.; Wang, S. L.; Zhu, L.; Wu, P. Y.; Dai, W. B.; Rakesh, K. P. Structure-activity relationship (SAR) studies of synthetic glycogen synthase kinase-3 β inhibitors: A critical review. *Eur. J. Med. Chem.* **2019**, *164*, 448–470.
- (35) Saraswati, A. P.; Hussaini, S. M. A.; Krishna, N. H.; Babu, B. N.; Kamal, A. Glycogen synthase kinase-3 and its inhibitors: potential target for various therapeutic conditions. *Eur. J. Med. Chem.* **2018**, *144*, 843–858.
- (36) Khan, I.; Tantray, M. A.; Alam, M. S.; Hamid, H. Natural and synthetic bioactive inhibitors of glycogen synthase kinase. *Eur. J. Med. Chem.* **2017**, *125*, 464–477.
- (37) Palomo, V.; Martinez, A. Glycogen synthase kinase 3 (GSK-3) inhibitors: a patent update (2014–2015). *Expert Opin. Ther. Pat.* **2017**, *27*, 657–666.
- (38) Gentles, R. G.; Hu, S.; Dubowchik, G. M. Chapter 1 Recent advances in the discovery of GSK-3 inhibitors and a perspective on their utility for the treatment of Alzheimer's disease. In *Annual Reports in Medicinal Chemistry*; Elsevier, 2009; Vol. 44, pp 3–26.
- (39) Augello, G.; Emma, M. R.; Cusimano, A.; Azzolina, A.; Montalto, G.; McCubrey, J. A.; Cervello, M. The role of GSK-3 in cancer immunotherapy: GSK-3 inhibitors as a new frontier in cancer treatment. *Cells* **2020**, *9*, 1427.
- (40) Taylor, A.; Rudd, C. E. Small Molecule Inhibition of Glycogen Synthase Kinase-3 in Cancer Immunotherapy. In *Human Cell Transformation, Advances in Experimental Medicine and Biology*; Rhim, J. S.; Dritschilo, A.; Kremer, R., Eds.; Springer Nature Switzerland: Cham, Switzerland, 2019; Vol. 1164, pp 225–233.
- (41) Lovestone, S.; Boada, M.; Dubois, B.; Hüll, M.; Rinne, J. O.; Huppertz, H.-J.; Calero, M.; Andrés, M. V.; Gómez-Carrillo, B.; León, T.; del Ser, T. A phase II trial of tideglusib in Alzheimer's disease. *J. Alzheimer's Dis.* **2015**, *45*, 75–88.
- (42) Selenica, M.-L.; Jensen, H. S.; Larsen, A. K.; Pedersen, M. L.; Helboe, L.; Leist, M.; Lotharius, J. Efficacy of small-molecule glycogen synthase kinase-3 inhibitors in the postnatal rat model of tau hyperphosphorylation. *Br. J. Pharmacol.* **2007**, *152*, 959–979.
- (43) Saitoh, M.; Kunitomo, J.; Kimura, E.; Iwashita, H.; Uno, Y.; Onishi, T.; Uchiyama, N.; Kawamoto, T.; Tanaka, T.; Mol, C. D.; Dougan, D. R.; Textor, G. P.; Snell, G. P.; Takizawa, M.; Itoh, F.; Kori, M. 2-[3-[4-(Alkylsulfinyl)phenyl]-1-benzofuran-5-yl]-5-methyl-1,3,4-oxadiazole derivatives as novel inhibitors of glycogen synthase kinase-3 β with good brain permeability. *J. Med. Chem.* **2009**, *52*, 6270–6286.
- (44) Onishi, T.; Iwashita, H.; Uno, Y.; Kunitomo, J.; Saitoh, M.; Kimura, E.; Fujita, H.; Uchiyama, N.; Kori, M.; Takizawa, M. A novel glycogen synthase kinase-3 inhibitor 2-methyl-5-(3-{4-[*S*]-methylsulfinyl]phenyl}-1-benzofuran-5-yl)-1,3,4-oxadiazole decreases tau phosphorylation and ameliorates cognitive deficits in a transgenic model of Alzheimer's disease. *J. Neurochem.* **2011**, *119*, 1330–1340.
- (45) Uno, Y.; Iwashita, H.; Tsukamoto, T.; Uchiyama, N.; Kawamoto, T.; Kori, M.; Nakanishi, A. Efficacy of a novel, orally active GSK-3 inhibitor 6-methyl-N-[3-[[3-(1-methylethoxy)propyl] carbamoyl]-1H-pyrazol-4-yl]pyridine-3 carboxamide in tau transgenic mice. *Brain Res.* **2009**, *1296*, 148–163.
- (46) Fukunaga, K.; Uehara, F.; Aritomo, K.; Shoda, A.; Hiki, S.; Okuyama, M.; Usui, Y.; Watanabe, K.; Yamakoshi, W.; Kohara, T.; Hanano, T.; Tanaka, H.; Tsuchiya, S.; Sunada, S.; Saito, K.-I.; Eguchi, J.; Yuki, S.; Asano, S.; Tanaka, S.; Mori, A.; Yamagami, K.; Baba, H.; Horikawa, T.; Fujimura, M. 2-(2-Phenylmorpholin-4-yl)pyrimidin-4(3*H*)-ones; a new class of potent, selective and orally active glycogen synthase kinase-3 β inhibitors. *Bioorg. Med. Chem. Lett.* **2013**, *23*, 6933–6937.
- (47) Fukunaga, K.; Sakai, D.; Watanabe, K.; Nakayama, K.; Kohara, T.; Tanaka, H.; Sunada, S.; Nabeno, M.; Okamoto, M.; Saito, K.-I.; Eguchi, J.-I.; Mori, A.; Tanaka, S.; Inazawa, K.; Horikawa, T. Discovery of novel 2-(alkylmorpholin-4-yl)-6-(3-fluoropyridin-4-yl)-pyrimidin-4(3*H*)-ones as orally-active GSK-3 β inhibitors for Alzheimer's disease. *Bioorg. Med. Chem. Lett.* **2015**, *25*, 1086–1091.
- (48) Berg, S.; Bergh, M.; Hellberg, S.; Höglin, K.; Lo-Alfredsson, Y.; Söderman, P.; von Berg, S.; Weigelt, T.; Ormö, M.; Xue, Y.; Tucker, J.; Neelissen, J.; Jerning, E.; Nilsson, Y.; Bhat, R. Discovery of novel potent and highly selective glycogen synthase kinase-3 β (GSK3 β) inhibitors for Alzheimer's disease: design, synthesis, and characterization of pyrazines. *J. Med. Chem.* **2012**, *55*, 9107–9119.
- (49) Sivaprakasam, P.; Han, X.; Civello, R. L.; Jacutin-Porte, S.; Kish, K.; Pokross, M.; Lewis, H. A.; Ahmed, N.; Szapiel, N.; Newitt, J. A.; Baldwin, E. T.; Xiao, H.; Krause, C. M.; Park, H.; Nophsker, M.; Lippy, J. S.; Burton, C. R.; Langley, D. R.; Macor, J. E.; Dubowchik,

- G. M. Discovery of new acylaminopyridines as GSK-3 inhibitors by a structure guided in-depth exploration of chemical space around a pyrrolopyridinone core. *Bioorg. Med. Chem. Lett.* **2015**, *25*, 1856–1863.
- (50) Luo, G.; Chen, L.; Burton, C. R.; Xiao, H.; Sivaprakasam, P.; Krause, C. M.; Cao, Y.; Liu, N.; Lippy, J.; Clarke, W. J.; Snow, K.; Raybon, J.; Arora, V.; Pokross, M.; Kish, K.; Lewis, H. A.; Langley, D. R.; Macor, J. E.; Dubowchik, G. M. Discovery of isonicotinamides as highly selective, brain penetrable, and orally active glycogen synthase kinase-3 inhibitors. *J. Med. Chem.* **2016**, *59*, 1041–1051.
- (51) Luo, G.; Chen, L.; Jacutin-Porte, S.; Han, Y.; Burton, C. R.; Xiao, H.; Krause, C. M.; Cao, Y.; Liu, N.; Kish, K.; Lewis, H. A.; Macor, J. E.; Dubowchik, G. M. Structure–activity relationship (SAR) studies on substituted *N*-(pyridin-3-yl)-2-amino-isonicotinamides as highly potent and selective glycogen synthase kinase-3 (GSK-3) inhibitors. *Bioorg. Med. Chem. Lett.* **2023**, *81*, No. 129143.
- (52) Ulrich, R. G.; Bacon, J. A.; Brass, E. P.; Cramer, C. T.; Petrella, D. K.; Sun, E. L. Metabolic, idiosyncratic toxicity of drugs: overview of the hepatic toxicity induced by the anxiolytic, panadol. *Chem. Biol. Interact.* **2001**, *134*, 251–270.
- (53) (a) Luo, G.; Chen, L.; Dubowchik, G. M.; Jacutin-Porte, S. E.; Vrudhula, V. M.; Pan, S.; Sivaprakasam, P.; Macor, J. E. GSK-3 inhibitors. World Patent Appl. WO2015/069594 A1, 2015. (b) Luo, G.; Chen, L.; Jacutin-Porte, S.; Burton, C. R.; Xiao, H.; Sivaprakasam, P.; Krause, C. M.; Cao, Y.; Liu, N.; Nophsker, M.; Snow, K.; Clarke, W. J.; Raybon, J.; Arora, V.; Pieschl, R.; Baireedy, P.; Wojcik, T.; Li, Y.-W.; Tian, Y.; Hong, Y.; Bryce, D.; Snyder, B.; Keenan, S.; Devidze, N.; Lidge, R.; Easton, A.; Kish, K.; Lewis, H. A.; Macor, J. E.; Dubowchik, G. M. Discovery of *N*-(4-phenylpyridin-3-yl)-2-((5-(trifluoromethyl)pyridin-2-yl)amino)isonicotinamide (BMS-743), a highly selective, brain penetrable and orally active inhibitor of glycogen synthase kinase-3 (GSK-3) for the potential treatment of Alzheimer's disease. Manuscript in preparation.
- (54) Schrödinger Release 2020-1: Maestro; Schrödinger, LLC: New York, NY, 2019.
- (55) The PyMOL Molecular Graphics System, version 2.3.2; Schrödinger LLC.
- (56) Hitchcock, S. A.; Pennington, L. D. Structure–brain exposure relationships. *J. Med. Chem.* **2006**, *49*, 7559–7583.
- (57) Ahmed, M.; Briggs, M. A.; Bromidge, S. M.; Buck, T.; Campbell, L.; Deeks, N. J.; Garner, A.; Gordon, L.; Hamprecht, D. W.; Holland, V.; Johnson, C. N.; Medhurst, A. D.; Mitchell, D. J.; Moss, S. F.; Powles, J.; Seal, J. T.; Stean, T. O.; Stemp, G.; Thompson, M.; Trail, B.; Upton, N.; Winborn, K.; Witty, D. R. Bicyclic heteroarylpirazinines as selective brain penetrant 5-HT₆ receptor antagonists. *Bioorg. Med. Chem. Lett.* **2005**, *15*, 4867–4871.
- (58) The synthetic routes to the imidazo[1,2-*b*]pyridazines described herein were first disclosed in: Hartz, R. A.; Ahuja, V. T.; Sivaprakasam, P.; Dubowchik, G. M.; Macor, J. E. GSK-3 inhibitors. World Patent Appl. WO2018/098411 A1, 2018.
- (59) The experimental procedures for the preparation of the 3-aminopyridine intermediates that were not commercially available were either previously described in refs 50 and 51 or are included in the Supporting Information.
- (60) Karaman, M. W.; Herrgard, S.; Treiber, D. K.; Gallant, P.; Atteridge, C. E.; Campbell, B. T.; Chan, K. W.; Ciceri, P.; Davis, M. I.; Edeen, P. T.; Faraoni, R.; Floyd, M.; Hunt, J. P.; Lockhart, D. J.; Milanov, Z. V.; Morrison, M. J.; Pallares, G.; Patel, H. K.; Pritchard, S.; Wodicka, L. M.; Zarrinkar, P. P. A quantitative analysis of kinase inhibitor selectivity. *Nat. Biotechnol.* **2008**, *26*, 127–132.
- (61) The IC₅₀ value of 47 for the following kinases is >2.0 μM: AURORA-B, BMX, BTK, CK2A1, CK2A2, IRAK1, IRAK4, ITK, JAK1, JAK2, LCK, LynA, p38α, SYK, TEC, TXK, and TYK2. The IC₅₀ value of 47 for the following kinases is >50 μM: cKIT, IGF1R, mAurA, MK2, PDGFRβ, and RSK1.
- (62) cLogP values were calculated using ChemDraw Professional 16.0.
- (63) Estimation of the topological polar surface area (tPSA) was calculated using the ChemAxon software (<https://docs.chemaxon.com/display/docs/polar-surface-area-plugin-2d.md>), which is based on the method described in: Ertl, P.; Rohde, B.; Selzer, P. Fast calculation of molecular polar surface area as a sum of fragment-based contributions and its application to the prediction of drug transport properties. *J. Med. Chem.* **2000**, *43*, 3714–3717.
- (64) LE was calculated using $(1.37/\text{HA}) \times \text{GSK-3}\beta \text{ pIC}_{50}$ (HA = number of non-hydrogen atoms). LLE values were calculated using GSK-3β pIC₅₀ – cLogP (reported in Table 5). More details regarding these calculations are described in: Hopkins, A. L.; Keserü, G. M.; Leeson, P. D.; Rees, D. C.; Reynolds, C. H. The role of ligand efficiency metrics in drug discovery. *Nat. Rev. Drug Discovery* **2014**, *13*, 105–121.
- (65) Fagerberg, J. H.; Tsinman, O.; Sun, N.; Tsinman, K.; Avdeef, A.; Bergström, C. A. S. Dissolution rate and apparent solubility of poorly soluble drugs in biorelevant dissolution media. *Mol. Pharmaceutics* **2010**, *7*, 1419–1430.
- (66) Liu, X.; Wright, M.; Hop, C. E. C. A. Rational use of plasma protein and tissue binding data in drug design. *J. Med. Chem.* **2014**, *57*, 8238–8248.
- (67) Rowland, M. Protein binding and drug clearance. *Clin. Pharmacokinet.* **1984**, *9*, 10–17.
- (68) Oddo, S.; Caccamo, A.; Shepherd, J. D.; Murphy, M. P.; Golde, T. E.; Kayed, R.; Metherate, R.; Mattson, M. P.; Akbari, Y.; LaFerla, F. M. Triple-transgenic model of Alzheimer's disease with plaques and tangles: intracellular Aβ and synaptic dysfunction. *Neuron* **2003**, *39*, 409–421.
- (69) Kieltyka, K.; Zhang, J.; Li, S.; Vath, M.; Baglieri, C.; Ferraro, C.; Zvyaga, T. A.; Drexler, D. M.; Weller, H. N.; Shou, W. Z. A high throughput bioanalytical platform using automated infusion for tandem mass spectrometric method optimization and its application in a metabolic stability screen. *Rapid Commun. Mass Spectrom.* **2009**, *23*, 1579–1591.
- (70) Cai, X.; Madari, S.; Walker, A.; Paiva, A.; Li, Y.; Herbst, J.; Shou, W.; Weller, H. Addition of optimized bovine serum albumin level in a high-throughput Caco-2 assay enabled accurate permeability assessment for lipophilic compounds. *SLAS Discovery* **2019**, *24*, 738–744.
- (71) Cai, X.; Walker, A.; Cheng, C.; Paiva, A.; Li, Y.; Kolb, J.; Herbst, J.; Shou, W.; Weller, H. Approach to improve compound recovery in a high-throughput Caco-2 permeability assay supported by liquid chromatography–tandem mass spectrometry. *J. Pharm. Sci.* **2012**, *101*, 2755–2762.
- (72) Experimental UPLC–MS/MS analysis details are included in Table S3 in the Supporting Information section.